Indoor Positioning

Bluetooth Angle of Arrival

KHADEEJA ATTEYA
MOHAMMAD AMER
MASTER´S THESIS
DEPARTMENT OF ELECTRICAL AND INFORMATION TECHNOLOGY
FACULTY OF ENGINEERING | LTH | LUND UNIVERSITY

Indoor Positioning

Bluetooth Angle of Arrival

Khadeeja Atteya
(khadeeja.atteya@gmail.com)
Mohammad Amer
(mohm-amer@hotmail.com)

Lund University

2019

Under supervision of

Ove Edfors

Professor of Radio systems at Lund University

Henrik Sihm

Head of Innovation department at Sigma Connectivity

Examined by

Fredrik Rusek

Associate Professor at Lund University

Lund University
Faculty of Engineering LTH
Department of Electrical and Information Technology
SE-22100 Lund, Sweden

Abstract

In this thesis, we present the Angle of Arrival (AoA) technique to detect the direction of a source indoors using radio frequency (RF) signal. This technique estimates the direction of the incoming Bluetooth signal, using a tag as a transmitter and an array equipped with a number of antennas as a receiver. We explore the theoretical basis of array processing and algorithms for direction finding. A simulation of the suggested direction finding algorithms was performed.
The main task of this thesis is to test and analyse a commercial widely-used Bluetooth-based indoor positioning system using angle of arrival technique. We explain the system architecture and characteristics. To evaluate the performance of the system, several experiments and testing have been implemented. Afterwards, we discuss the results gathered from these measurements and the reasons behind them.
The obtained results showed that there is a gap between the theoretical expectations and the empirical measurements in different environments. The main factors affecting the performance have been identified and analysed. We suggest that there can be room for enhancement.

Preface

This thesis project was carried out as a part of the International Master programme of Wireless Communication at Lund University, Department of Electrical and Information Technology, during the final semester of the programme between January and June 2019. It has been performed at the office and laboratories of Sigma Connectivity, Lund, Sweden. Sigma Connectivity is a leading consulting company, established in 2013, that is interested in investing in the field of communication and Internet of Things (IoT). Indoor positioning is among their field of interest. Theoretical studies and measurements have taken place were done by both participants.

Acknowledgement

We would like to take this chance to thank the opportunity given to us by Lund University as an entity of higher education. Additionally, to express our appreciation for the effort done by all its employees and personnel to ensure a suitable environment for international studies in an atmosphere that encourages diversity and initiation. We appreciate that students can have a fair equal opportunity regardless of their nationality, skin colour, gender or any other aspects. Special thanks goes to both Professor Ove Edfors at LTH and Henrik Sihm at Sigma Connectivity for their support and mutual understanding as our thesis supervisors.

Khadeeja Atteya
Mohammad Amer

Popular science summary

Positioning is the concept of estimating the position of an object. In this thesis, we use radio waves as the means.

Internet of Things (IoT) is an umbrella term used to describe connecting everyday objects to the internet. The number of connected devices to the internet is increasing dramatically. This success in the IoT field has increased the need for different wireless communication-based applications. Indoor positioning is among the applications that have attracted attention for many years; since the detection of objects positions in hospitals, stadiums and malls, *etc* has become an important part of daily life. There are different techniques and systems that can be used to design an efficient indoor positioning system (IPS).

Bluetooth Low Energy (BLE) is a relatively new and very attractive technology to use due to its availability in smart devices and low power consumption. The angle of arrival (AoA) estimation technique has been chosen as the receiver is not very complex to build and still gives an acceptable accuracy. AoA is a direction-finding technique that exploits the impinging angles of arriving signals at antenna array in the receiver side. Based on these angles, the phase difference of received signals between two antennas can be found and used by direction finding algorithms to estimate target position.

In this thesis, a commercial indoor positioning system (IPS) has been studied, analysed and tested. With the goal of understanding the key factors of the accuracy level, testing scenarios in different indoor environments have been conducted. The results have shown that the accuracy level is still behind the expectations with an accuracy of +/-4 degrees from the actual angle. In this thesis, the reasons for that were discussed, and some suggestions were given to improve the system performance. When designing an IPS, there are principle causes of error that need to be identified and tackled. Receiver noise, error resulting from analog-to-digital conversion (ADC) and wave components due to reflections, *i.e.* multipath components (MPC). Error caused by noise can be controlled by keeping a reasonable level of transmitter signal power. Higher quality hardware can minimize sampling error or the error caused by ADC. MPC can cause high error in estimation, far from the actual position. This type of error can be reduced by choosing a suitable algorithm. Higher transmitting power, quality hardware and complex algorithms come with cost. Commercial IPS manufacturers have to do a trade-off between the financial cost and system performance. There is a "sweet spot" that can be found for all the factors stated above so that they can altogether give an acceptable estimation, at a reasonable price. Finding this sweet spot for each factor is essentially a business decision. On the other hand, the environment where the system is used affects the performance on a large scale. A system can operate reasonably well in a static environment, for example, a large room with not so many objects that may cause reflected waves and disturb the position estimation. However, the same system may function poorly if there are many reflectors; such as metal objects and narrow passages. For future work, a flexible system can be designed to perform with dynamic specifications depending on the environment it is being used.

List of Abbreviations

1-D One dimension

2-D Two dimension

3-D Three dimension

ADC Analog to Digital Conversion

AoA Angle of Arrival

AoD Angle of Departure

AWGN Additive White Gaussian Noise

BLE Bluetooth Low Energy

BR Basic Rate

CRC Cyclic Redundancy Check

CSMA/CA Carrier Sense Multiple Access/Collision Avoidance

CTE Constant Tone Extension

DoA Direction of Arrival

DoD Direction of Departure

DQPSK Differential Quadrature Phase Shift Keying

EDR Enhanced Data Rate

EVD Eigenvalue Decomposition

GFSK Gaussian Frequency Shift Keying

GHz Giga Hertz

GNSS Global navigation satellite system

GPS Global Positioning System

HF High Frequency

IEEE Institute of Electrical and Electronic Engineers

IID independet and identically distributed

IoT Internet of Things

IPS Indoor Positioning System

ISM Industrial Scientific and Medical

kbps kilobits per second

LE Low Energy

LoS Line of Sight

MAI Multiple Access Interference

MCU Micro-controller Unit

MISO Multiple Input Single Output

MPC Multipath Component

Mbps Megabits per second

PC Personal Computer

PHY Physical Layer

PSK Phase Shift Keying

RF Radio Frequency

RFID Radio Frequency Identification

RSS Received Signal Strength

RSSI Received Signal Strength Indicator

RTLS Real-Time Location System

RToF Round-trip Time of Flight

SIMO Single Input Multiple Output

SNOI Signal Not of Interest

SNR Signal to Noise Ratio

SOI Signal of Interest

SVD Singular Value Decomposition

TDD Time Division Duplex

TDoA Time Difference of Arrival

ToF Time of Flight

QPSK Quadrature Phase Shift Keying

UCA Uniform Circular array

ULA Uniform Linear Array

UWB Ultra Wide Band

WiFi Wireless Fidelity

WLAN Wireless Local Area Network

WPAN Wireless Personal Area Network

List of Figures

List of Tables

Contents

Chapter 1

Introduction

1.1 Motivation

For the past few years, Internet of Things (IoT) and its applications have become one of the hot topics in the field of wireless communications. Not only that it facilitates a large variety of ways and forms to control different devices and through many platforms, but also such applications can be performed with low power consumption. Positioning and direction finding are some of the top applications of IoT.

The continuous growth in wireless communication technology opened the door widely for many applications such as positioning. Positioning has always been in people's thoughts throughout history, tracing back to the old days when people used to follow the ancient guiding-star navigation. Since then, a lot of technological growth has been seen and satellite-based systems have practically solved the problem of outdoor localization. Due to the difference in nature between indoor and outdoor environments, the techniques used outdoors cannot always perform with the same accuracy indoors. Outdoor positioning systems limitations lead to a challenge of developing a new system for indoor environments [1]. Yet, the demand for accurate position detection in the indoor environment increased dramatically. Different industry sectors – such as hospitals manufactures, and malls, *etc* – show a high interest in this technology. Till now there is no particular standard system designed for indoor positioning [2].

1.2 Objective and Method

The aim of this project is evaluate the performance of a Bluetooth angle-of-arrival-based indoor positioning system (IPS) and find the key factors that affect the sys-

tem performance. To reach our objective, we will study the theoretical background of antenna array processing and different angle of arrival (AoA) estimation algorithms. In addition, we will perform practical measurements on a commercial IPS and analyse the result, in order to suggest enhancements for future work, keeping in mind the commercial aspect. We are aware that the trade off between performance and cost is a challenge in any commercial communication system. Therefore, our proposed enhancements can be implemeted in a relatively low cost.

1.3 Structure of the thesis

This thesis consists of 6 chapters.This is Chapter 1, which is an introduction to this thesis. Next, Chapter 2 explains the positioning technologies and techniques that can be used to design an indoor positioning system. Then, Chapter 3 gives a theoretical description of the antenna array, AoA technique, and estimation algorithms. Chapter 4 presents the analysis of the indoor positioning systems that we analyse, mainly hardware and software(system algorithm) analysis. Afterwards, Chapter 5 presents the empirical measurements and shows the comparison of different criteria in different environments for two system setups. Finally, Chapter 6 summarises the results and suggestions for future work.

Chapter 2

Indoor positioning

This chapter presents the positioning systems (technologies) and techniques that can be used in indoor positioning. It starts by introducing the technologies and ends with the techniques, showing their features, weaknesses and how they can be applied in indoor positioning.

2.1 Positioning systems

When choosing a technology for an indoor positioning system (IPS), some trade-offs have to be made; such as accuracy, coverage range and cost among others. Figure 2.1 summarizes the accuracy versus coverage range comparison. The advantages and disadvantages of the most common technologies are discussed and we justify our choice of Bluetooth Low Energy (BLE).

- **Global Navigation Satellite System (GNSS)** GNSS is a generic name for a group of satellite-based positioning systems. Satellite-Based positioning systems send geospatial information to receivers to determine locations. Examples of different GNSS's are:
  - Global Positioning System (GPS) refers to the satellite system created by the USA. The terms GNSS and GPS are often used interchangeably.
  - Galileo is a global outdoor positioning system created by the European Union and the European Space Agency.
  - GLONASS (Global Navigation Satellite System) is the Russian navigation system.
  - BeiDou-2 or BDS is the navigation system created by China.

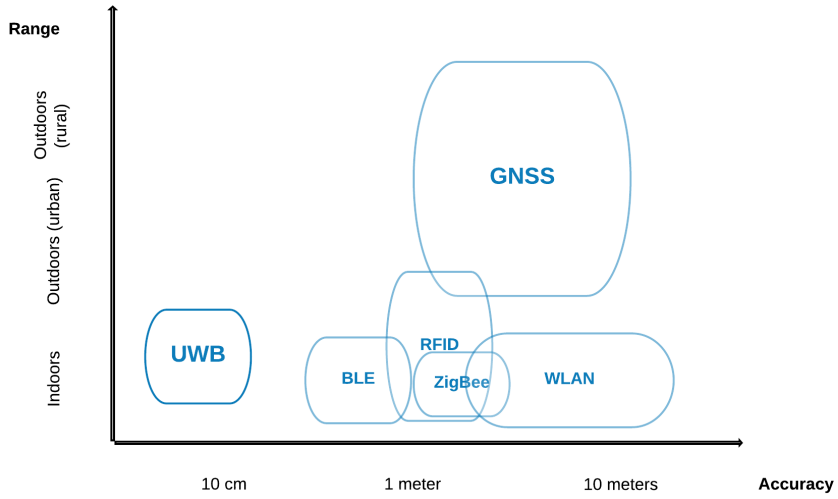

Figure 2.1: Range and accuracy of common positioning systems.

A satellite-based positioning system typically works outdoors with the possibility to achieve accuracy level up to 5 meters. However, it does not work as well indoors due to blockage of satellite signals by different obstacles such as walls, since the system depends on LOS (line of sight) signals. GNSS systems depend on finding an intersection point between 3 circles estimated by 3 satellites, which is called" trilateration" (the concept of trilateration is explained in Chapter 3). Satellite-based systems are quite complex and require complicated receivers and relatively high costs. Therefore, purchasing rights to use and utilize positioning information for business use can be considered an unwise financial decision. [2], [3].

- **Radio Frequency Identification (RFID)**

  RFID is primarily intended for transferring and storing data using an electromagnetic transmission from a transmitter to any Radio Frequency (RF) compatible circuit [4]. As explained in [4], RFID systems are represented by a tag (transmitter) and a reader (receiver). Pre-defined RF protocol known to the transmitter and receiver used by the receiver for communicating. RFID is divided into two types:

  - Active RFID: this type is considered a long communication range as

it can cover up to hundreds of meters. It uses microwave frequency. It could be an option to use in positioning since it is not relatively expensive and has a good coverage range. However, it is not usually used in indoor positioning due to its low accuracy. In addition, it is not usually found in common end-user devices.

- Passive RFID: this type also operates on microwave frequencies. Its main advantages are that it requires small-size and light-weight transmitters and receivers and does not require a battery. However, the coverage range is short (1-2 meters). That is why it cannot be a good candidate for indoor positioning.

- **Ultra-Wide Band (UWB)**

UWB positioning is based on sending ultrashort pulses (usually in nanoseconds) which would occupy a large spectrum -more than 500 MHz wide. It transmits a signal over a large frequency band between 3.1 to 10.6 GHz. The shorter the pulse, the larger bandwidth it occupies, as appears in Figures 2.2 and 2.3. The accuracy of an UWB positioning system comes directly from how short the pulses are. The short pulses simplify the filtration process between the actual signal and the multipath signal. That is how UWB system can be *immune* to NLOS (non-line-of-sight) components, thus, higher accuracy with fine time resolution [3], [5].

Low power consumption and the ability to work across a broad spectrum range are the main features that distinguish UWB. The accuracy of UWB is high since it has precise synchronization of the Time of Arrival (TOA) technique. However, it is not widely applied in indoor positioning because most of the end-user devices don't have UWB chips. Besides, UWB positioning devices are quite expensive. UWB kits have a price range of a few thousand Euros (ranging around 1000 to 4000) [6],[7].

- **Wireless Local Area Network (WLAN)**

WLAN operates on different frequency bands, among them ISM (Industrial Scientific and Medical) frequency band 2.4GHz and 5GHz, which are the bands that are of concern for positioning in WLAN. WLAN mainly uses the Received Signal Strength Indicator (RSSI) for positioning. It can achieve an accuracy level of 3 to 30 meters. Furthermore, it can be used with different

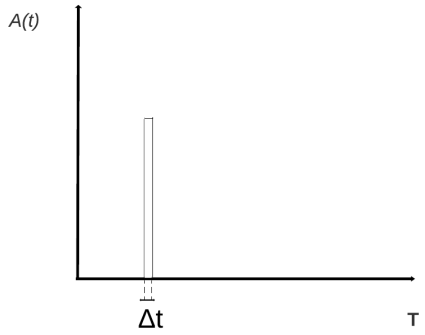

Figure 2.2: UWB pulse (time domain).

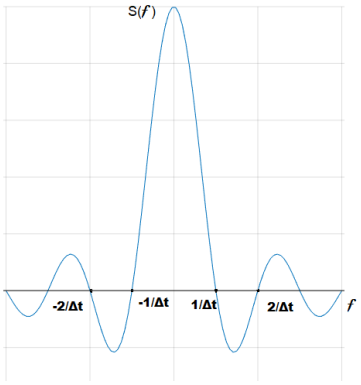

Figure 2.3: UWB pulse (freq- domain).

positioning techniques such as AoA and ToF. Due to its availability in current end-user devices (such as smartphones and laptops), it can be one of the best options for indoor positioning; in fact, WLAN is one of the most common indoor positioning technologies. However, it is not always the ideal candidate. WiFi is a system designed and primarily used for information and data exchange. It uses Carrier Sense Multiple Access with Collision Avoidance (CSMA/CA) protocol. In short, the packet checks if a channel is clear before transmission. In case it is not clear, the transmitter 'waits' a randomly chosen period of time before trying to check the channel again. The nature of this protocol may cause an enormous delay when being used for positioning, especially in a heavy-traffic network. Still, there are other drawbacks such as high fluctuation in RSSI level due to the effect on signal caused by the indoor environment structure *i.e.* multipath components and co-channel interference since there can be other wireless routers operating on the same frequency [4], [8], [9].

- **ZigBee**

ZigBee is a wireless technology standard that can be regarded as a low rate Wireless Personal Area Network (WPAN). It is based on IEEE 802.15.4 specification and operating in the unlicensed ISM frequency bands at 2.4 GHz and sub-GHz. Zigbee is an RSS-based mesh network as appears in Figure 2.4 . Typically, it contains three types of devices: coordinator, router and end device (transmitter). The network has one coordinator and a number of routers, together they estimate the end device's position. Since it is low-power, low-cost, has a coverage range up to 30m with accuracy that

can reach 3 meters-level. Zigbee is a good candidate to be used in indoor positioning. However, practically it is not preferred due to its unavailability in most end-user devices and its architecture complexity [4], [5], [10].

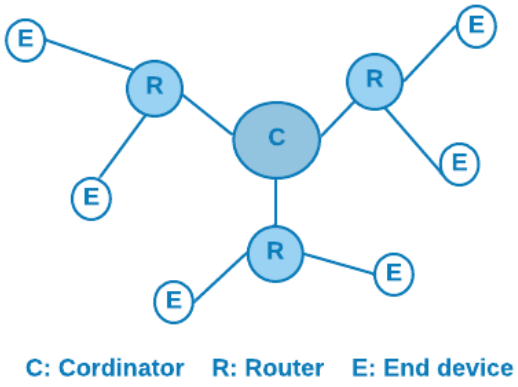

Figure 2.4: ZigBee mesh network illustration.

- **Bluetooth Low Energy (BLE)**

  BLE is one of the most famous wireless technologies. It operates in the 2.4 GHz ISM frequency band. It has caught attention for the past years. It is embedded in the majority of electronic devices such as smartphones, laptops, *etc*. BLE has a short coverage range and low data rate. As it consumes low energy, it is an attractive technology to be used with different positioning techniques such as AoA, RSS, ToF, *etc*. In addition, it can achieve an accuracy level of sub-meter. Therefore, it is suitable for IoT applications that require minimal human interaction to handle power supply.

  A new feature for direction finding has been added to BLE 5.1. The addition of the direction finding feature is the first of several steps in the Bluetooth roadmap that will ultimately enable key enhancements to Bluetooth location services. When the associated profiles have been released, Bluetooth developers will be able to exploit the new direction finding controller capability to create high accuracy for positioning systems such as real-time locating systems (RTLS) and IPS [4], [11]. These reasons make Bluetooth an attractive technology for indoor positioning. We discuss Bluetooth in detail in Chapter 4.

Table 2.1 summarizes the above, showing the main advantages and disadvantages

of the main positioning technologies.

Technology	Maximum range(m)	Maximum throughput	Power consumption	Cost	Accuracy level
RFID	200	low	low		1-2 m
UWB	20	460 Mbps	low	high	10-20 cm
ZigBee	30		very low	low	3m
WLAN	35	1.3 Gbps	moderate	low	3-30 m
Bluetooth	100	24 Mbps	low	low	sub-meter

Table 2.1: Comparison between different positioning technologies [4].

2.2 Positioning techniques

Received signal strength (RSS), time difference of arrival (TDoA), time of arrival (ToA), and angle of arrival (AoA) are the main techniques used in positioning that we discuss and compare to explain the reason that AoA technique was chosen.

- **Received Signal Strength (RSS)**

  RSS is one of the main used techniques for indoor positioning. It depends on measuring the received signal power. The strength of the received signal depends on the propagation environment and distance between transmitter and receiver. Signal power decays gradually as the signal goes further from the transmitter. The relation between power and distance is represented by path loss. The combination of this information with a propagation model can help to determine the distance between the transmitter and receiver. Simplicity and low cost of implementation are the main features of RSS. Yet, its positioning accuracy level is rather poor, in particular in non-line of sight (NLOS) situations due to multipath propagation [2]. Path loss can be defined as the ratio between the received and transmitted power, taking into account the system's other losses and gains (*i.e. link budget*). In free space, the path loss – between isotropic antennas – is proportional to the distance squared as per

  $$pathloss = (\frac{4\pi d}{\lambda})^2, \tag{2.1}$$

  where d is the separation between the transmitter and the receiver and λ is the wavelength of the signal. With prior knowledge of the received power value at one meter distance, we can estimate the distance d_o from

  $$P_r(d_o) = P_r(1m) - 20\log(d_o), \tag{2.2}$$

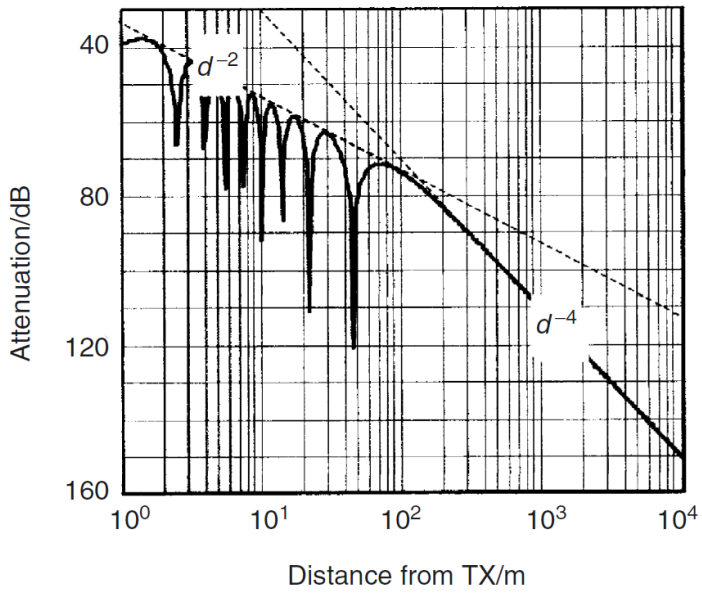

Figure 2.5: Propagation over an ideally reflecting ground [12].

where $P_r(d_o)$ is the received power at distance d_o and $P_r(1m)$ is received power at 1 meter distance [12]. However, the path-loss exponent of 2 in (2.1), is for the path-loss in free space. Theoretically, over ideally reflecting ground, this exponent can vary from 2 to 4, as illustrated in Figure 2.5. However,in reality, it can vary much more than in theoretical situation as in complex building structure environments where the exponent can reach as high as 6. It can be tricky to determine the exponent precisely in an RSS-dependent positioning system, since the dependency on environment and distance require extra effort in channel modelling before designing such a system.

- **Time of Arrival (ToA)**

  The precise measurement of signal arrival time to reference nodes is the main base for the ToA technique. In ToA, the transmitter sends a time-stamped signal towards receiving nodes. From the received signal, the transmission time delay and the speed of the signal (*i.e.* the speed of light) can be measured and used to find the distance between the target and the reference nodes. Accurate synchronization between the transmitter and the reference nodes is a critical requirement as the transmission start-time is the base for ToA technique. With precise synchronization, ToA is one of the most accurate techniques. That is why it is used in most satellite-based po-

sitioning systems. Yet, to achieve that requirement, a certain type of clocks (such as atomic clocks) must be used. Therefore, TOA-based systems are considered to be a challenge to be used an IPS [4].

- **Time Difference of Arrival (TDoA)**

  TDoA is based on measuring the transmission time difference of the received signal from three known reference nodes. Accurate synchronization between reference nodes with each other is necessary, but it is not required between the transmitter and reference nodes as in ToA. Synchronization between nodes is easier to achieve through the core network. Suppose there are 3 reference nodes, node A, B and C, and one transmitter as shown in Figure 2.6. The reception time is T_a, T_b, and T_c. Finding the time difference between each pair of nodes, the corresponding difference in distance, three distances can be calculated:

$$\Delta d_1 = c(T_a - T_b),$$
$$\Delta d_2 = c(T_b - T_c),$$
$$\Delta d_3 = c(T_a - T_c).$$

  where c is the speed of light. Using the three calculated distances differences $\Delta d_1, \Delta d_2$ and Δd_3, the position can be estimated.

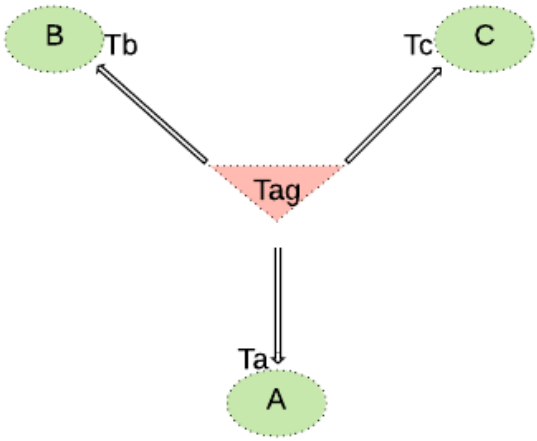

Figure 2.6: TDoA overview.

Avoidance of synchronization between transmitter and receiver and focusing only on synchronization between reference nodes is one of the main

advantages of TDoA. This guarantees minimizing measurement error since arrival time error -due to mis-synchronization- will be the same for all reference nodes. On the other hand, clock synchronization between reference nodes is not a simple process and it still adds more complexity [5].

- **Direction finding (Angle-based positioning)**

  All the prior techniques aimed mainly to estimate the position of an object by estimating the distance between the object and a reference node. Direction finding techniques estimate the position of an object by measuring the angle of the incoming/departing signal from/to this object. It is divided into two types:

  1. Angle of Arrival (AoA), also referred to as Direction of Arrival (DoA): a single antenna transmitter and a receiver (locator) equipped with an antenna array. This system is an example of a Single Input Multiple Output (SIMO) system. The object transmits signal beams that arrive at the locator as a planar wave front (in the far field). These beams do not arrive at the same time at different receiver antennas, as the durations they travel are varies depending on their impinging angles and the distance between antenna pairs. Differences in travelling time would cause phase differences of the signal impinging on the receiver between each antenna and its neighbours. Using the geometry of the antenna array at the receiver, we can calculate the AoA of the signal with respects to the receiver. More details on how this estimation is done are found in the next chapter.

  2. Angle of Departure (AoD), also referred to as Direction of Departure (DoD): the transmitter has an antenna array and the receiver has a single antenna, which is an example of a Multiple Input Single Output (MISO) system. Here, the roles are reversed. The transmitter transmits beams to a receiver and switches between the elements of the antenna array, *i.e.* each antenna transmits for a pre-decided period of time in sequence. Similarly to an AoA system, the signals transmitted from different antennas travel different distances and arrive at the receiver at different times causing phase differences in the impinging signals. With prior knowledge of the antenna switching at the transmitter, the receiver utilizes the difference in phase differences between the incoming signals from the different antenna elements to estimate its own – the receiver's – angle in relation to the transmitter. The receiver is still the locator, same as in an AoA system, but it locates itself, rather than other objects.

  As mentioned previously, both AoA and AoD systems operate similarly.

The main difference is the number of antennas on the transmitter and receiver sides. It depends on the application and the environment to decide which to use. For example, an AoA-based system can be used in an office or industrial environment to locate tools or equipment or locate a car in a parking lot/garage. An AoD example can be a mobile application that helps the user find their way in a building, where the locator pushes positioning information to the mobile phone- in a similar way that GNSS systems work. Direction finding- unlike previous techniques- does not require accurate synchronization between the transmitter and the receiver or costly resources such as wide bandwidth. For these reasons, direction finding techniques have become a very popular option among investing companies lately, which motivates the study performed here. In this thesis, we focus on AoA as a direction finding technique.

Chapter 3

Antenna Array Processing

This chapter explains the theoretical background of AoA. It starts by introducing antenna arrays, then the analysis of received signal at the antenna array and how the angles are calculated from a theoretical point of view. The remaining part of the chapter discusses examples of different algorithms of how the estimation of AoA is done and we compare them using simulations.

3.1 Antenna Arrays

Above we stated the reasons for favouring direction-finding over distance-finding techniques. The concept of estimating AoA or AoD is based on finding the phase difference between the received signals, as previously stated. A number of antennas connected together to an RF system (transmitter or receiver) form what is called an *antenna array*. Antenna arrays have become the basis for many communication systems, including IoT applications. In this section, we analyse the theoretical background of the antenna arrays.

Array processing consists of using multichannel observations collected by a sensor array in an optimal manner, in order to detect signals or to estimate their parameters [13]. From readings of [12], [13] and [14], we firstly state some conditions that apply to the signal model we describe later:

- Propagation medium is homogeneous, and distances between sources and antennas is large enough so that waves can be considered parallel and planar arriving at all antenna elements on the array.
- There are no sources of external interference, other than receiver noise.
- Only uncorrelated independent and identically distributed (IID) with zero

mean Additive white Gaussian noise (AWGN) at the array.

- The antenna array is stationary and the sources move slow enough to be considered stationary during one measurement, and no movements in the environment is interfering with the measurements.
- All sources are narrowband with only one incoming signal from each source.
- All antenna elements are ideal, identical, omnidirectional and equi-distantly spaced.
- All signal sources are orthogonal (with no correlation) to each other and uncorrelated to the noise (all sources can be analysed separately).

Since we depend mainly on the spatial position of the antenna elements in our case when estimating the direction of sources, the antenna geometry and other spatial features are of great concern. Here we focus on two examples of antenna arrays that are widely used in theoretical studies: Uniform Linear Array (ULA) and Uniform Circular Array (UCA).

3.1.1 Uniform Linear Array

A ULA is referred to as a 1-D array and is the case that we start with as it is considered to be the simplest form of antenna array. An antenna array is a spatial distribution of antennas in which the individual antennas are geometrically-identical, similarly-oriented, and energized at similarly-situated points. These properties ensure that the form of the current distribution is the same in all the elements of the array and that consequently the array is composed of antennas with the same radiation patterns. An array is linear if its points, similarly situated on the elements, are collinear [15]. This is how the author defined a ULA. From the basic definition stated above, we can conclude how beams arrive and interact with the array.

From the geometric features as shown in Figure 3.1, the time delay between each element and its neighbour will be

$$\tau = \frac{r}{c} = \frac{d \sin \phi}{c}, \tag{3.1}$$

where the extra distance that the wavefront travels is $r = d \sin \phi$, d is the separation between the antenna elements, c is the speed of the wave (*i.e.* the speed of light), which equals the product of the wavelength λ and the frequency f of the incident wave and ϕ is the angle of the wave with respect to the array as shown in Figure 3.1. The time delay results in a phase difference δ (assuming d is smaller than one wavelength), which can be expressed in terms of r so that

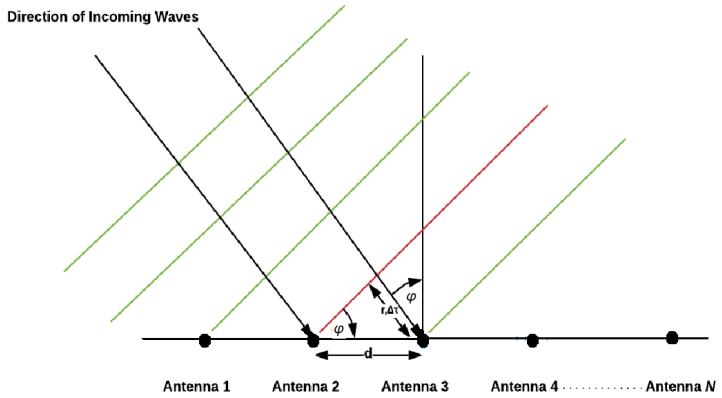

Figure 3.1: Geometric analysis of an N-element ULA.

$$\delta = 2\pi\frac{r}{\lambda} = 2\pi\frac{d\sin\phi}{\lambda}. \tag{3.2}$$

As mentioned above, all elements are equally-spaced, meaning that the time difference between each pair of neighbour antennas is equal. So, we express the phase difference through an N-element array as a *Vandermonde* vector to have what we would call the *array manifold vector* (*a.k.a. array steering vector*) and has the form

$$\mathbf{a}(\phi) = \left[1 \;\; e^{-j\frac{2\pi d}{\lambda}\sin\phi} \;\; e^{-j\frac{4\pi d}{\lambda}\sin\phi} \ldots \;\; e^{-j\frac{2(N-1)\pi d}{\lambda}\sin\phi}\right]^T. \tag{3.3}$$

The vector $\mathbf{a}(\phi)$ is the manifold vector for the antenna array, in case of having one source of signal, meaning one AoA (which is the unknown ϕ to be estimated). Therefore, when having D sources of signal, in other words having D angles to estimate. The *manifold matrix* would combine D manifold vectors as

$$\mathbf{A}(\phi) = [\mathbf{a}(\phi_1) \;\; \mathbf{a}(\phi_2) \;\; \ldots \;\; \mathbf{a}(\phi_D)], \tag{3.4}$$

where ϕ in $\mathbf{A}(\phi)$ is an angle parameter vector, containing all the individual ϕ_d angles. Accordingly, if one signal source is represented as $s_d(t)$ we can form the signal vector for D signal sources as

$$\mathbf{s}(t) = [\, s_1(t) \;\; s_2(t) \;\; \ldots \;\; s_D(t)]^T. \tag{3.5}$$

Now, we can form the ULA signal model to be

$$\mathbf{y}(t) = \mathbf{A}(\phi)\mathbf{s}(t) + \mathbf{n}(t), \tag{3.6}$$

where $\mathbf{y}(t)$ is the received signal vector by the antenna array and $\mathbf{n}(t)$ is the additive noise vector (as assumed before, we only have AWGN), that takes the form

$$\mathbf{n}(t) = [\, n_1(t) \;\; n_2(t) \;\; .... \;\; n_N(t)]^T. \tag{3.7}$$

3.1.2 Uniform Circular Array

The UCA is probably the most common 2-D antenna array shape due to its symmetry. Since the array manifold vector is dependent on the antenna geometry, we can conclude – in a similar way as above – the received signal vector for other shapes of antenna arrays only by manipulating the array manifold vector of the desired array, assuming that all condition stated previously apply. UCAs differ fundamentally from ULAs as the first have a 2-D shape. Assuming a planar view, ULA acts as a *mirror* on that plane, resulting in estimating two AoAs when only one signal impinges the ULA cause the estimation ambiguity. In other words, a beam impinging the ULA at angle ϕ, appears as both angles ϕ and $(2\pi - \phi)$ on the plane the ULA is placed. On the other hand, a UCA placed on a plane gives one AoA estimation for one incoming signal from any direction over the plane. Therefore, ULAs can practically "see" angles in the range $[0 : \pi]$ while UCAs can see all angles in the range of the entire plane $[0 : 2\pi]$. That is why UCAs have an advantage over ULAs by removing the ambiguity of the AoA estimation.

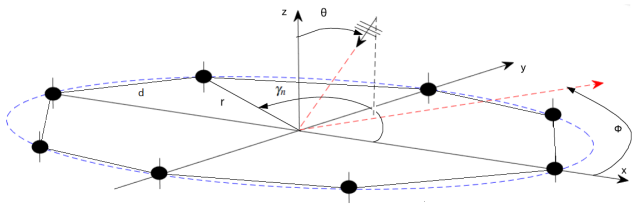

Figure 3.2: Uniform Circular Array.

Ideally, a UCA consists of N identical sensors evenly placed on a circle of radius r in the xy-plane as showin in Figure 3.2. The inter-element spacing is given by $d = 2r\sin\frac{\pi}{N}$ [13]. Here it is important – since we are analysing in 3-D – to define the *elevation* angle θ, alongside to the *azimuth* angle ϕ. In addition, we have another factor when defining the UCA elements, which is the inter-element angulation $\gamma_n = 2\pi\frac{n}{N}$ where $n = 0, 1, .., N-1$ which is usually "counted counter-clockwise from the x-axis" according to [16] and [17].

Assuming there is only one signal source, *i.e.* one azimuth angle ϕ and one elevation angle θ as illustrated in Figure 3.2, we can utilize the geometry of the circle to calculate the phase difference between the array element (for equation derivation, we refer the reader to [13], [14] and [18]). Assuming that the wavefront passes through the origin at time $t = 0$, it impinges on the nth element of the array at the relative time of [19]

$$\tau_n = \frac{r}{c} \sin\theta \cos(\phi - \gamma_n), \tag{3.8}$$

where r is the radius of the UCA, and c is the speed of light. We can also express the steering manifold vector of a UCA – using a "Vandermonde-like" structure – as

$$\mathbf{a}(\phi,\theta) = \left[e^{j\frac{2\pi r}{\lambda}\sin\theta\cos(\phi-\gamma_0)} \;\; e^{j\frac{2\pi r}{\lambda}\sin\theta\cos(\phi-\gamma_1)} \ldots e^{j\frac{2\pi r}{\lambda}\sin\theta\cos(\phi-\gamma_{N-1})} \right]^T. \tag{3.9}$$

Similarly to ULA, with D signal sources, the manifold matrix would have D columns. However, for simplicity of geometric analysis, we would assume at this point that all D sources are placed on the same plane, *i.e.* have the same elevation angle θ_0 and we would assume that θ_0 = 90 degrees. Now, we can re-write the steering manifold vector of the dth source to be

$$\mathbf{a}(\phi_d) = \left[e^{j\frac{2\pi r}{\lambda}\cos(\phi_d-\gamma_0)} \;\; e^{j\frac{2\pi r}{\lambda}\cos(\phi_d-\gamma_1)} \ldots e^{j\frac{2\pi r}{\lambda}\cos(\phi_d-\gamma_{N-1})} \right]^T. \tag{3.10}$$

So that, the manifold matrix would be the same as expressed in (3.4). Consequently, we have the same signal model that was previously expressed in (3.6)

Circular arrays have been used for many years in the HF band for both communications and direction finding [20]. Nevertheless, the advantages of uniform circular arrays come at a cost. Many useful array-processing techniques that are derived for uniform linear arrays do not extend directly to uniform circular arrays, due to the mathematical structure of their steering vector not possessing the convenient Vandermonde form [19].

3.2 Direction-finding algorithms

DoA estimation algorithms form the heart of smart antenna array systems. The goal behind using such algorithms is to extract transmitter position from raw data collected by the antenna array. There are different types of algorithms, depending on the way the AoA is estimated. Beam-space (*a.k.a.* beam-scan) algorithms are one type. Examples of this type are conventional and adaptive beamformers. Estimation of signal parameters via rotational invariant techniques (ESPRIT) and

Multiple Signal Classification (MUSIC) are widely used spectral estimation techniques, which fall under the category of subspace-based algorithms. This type of algorithms works on the principle of eigenvalue decomposition (EVD) of the covariance matrices [21].

3.2.1 Conventional beamformer

The sensors spatially sample the signal field at the locations of N-antenna elements, which yields a vector of source signals of size $Nx1$. We process each sensor output by a linear, time-invariant filter with impulse response $h_n(\tau)$, where

$$h_n(\tau) = \frac{1}{N}\delta(\tau + \tau_n). \tag{3.11}$$

As done in [14]. we get that by shifting the inputs from each sensor and adding a normalization factor as we have already assumed a time-invariant stationary channel. Therefore, the impulse response forms a vector that takes the form

$$\mathbf{h}(\tau) = [h_1(\tau)\ \ h_2(\tau)....h_N(\tau)]^T. \tag{3.12}$$

We assume that the observation interval is long enough that it may be considered infinite. Summing the outputs, we obtain the array output vector $\mathbf{y}(t)$ of size $Nx1$. This process is referred to as the **delay-and-sum beamformer** or the **conventional beamformer** [14].

Now, we can define the received signal $y(t)$ in terms of both time and angle of arrival. In our case, all antenna elements are equi-spaced *i.e.* we use the antenna placement so that

$$\mathbf{y}(t) = [y_1(t)\ \ y_2(t)....y_N(t)]^T. \tag{3.13}$$

From the previous definitions, we get the generalised received signal model as expressed in (3.6). For more detailed expressions and equations, the reader can refer to [14].

In this section, we are still assuming that the dominant source of error is AWGN (additive white Gaussian noise), added by the receiver antennas. The received signal is read by the antennas as *snapshots*, each of is represented by a vector of the received signal taken simultaneously at the uniformly spaced elements. The elements of each snapshot are called *samples*. For a single snapshot, the received signal vector is

$$\mathbf{y} = \mathbf{A}\mathbf{s} + \mathbf{n}, \tag{3.14}$$

where $\mathbf{s}$ is source signal vector, $\mathbf{n}$ is the noise vector, and $\mathbf{A}$ is the array manifold matrix representation. Keeping in mind that the AWGN is IID with zero mean,

the noise covariance matrix for K snapshots can be described by

$$\mathbf{R}_n = E\left[\mathbf{N}(k)\mathbf{N}(k)^H\right] = \sigma_\omega^2\mathbf{I}, \tag{3.15}$$

where $k = 1, 2, ..., K$, $E[\ ]$ refers to the expectation, $[\ ]^H$ refers to the *Hermitian transpose* of the matrix, σ_ω is the noise standard deviation and $\mathbf{I}$ is the identity matrix. As well, the signal covariance matrix would be defined as

$$\mathbf{R}_s = E\left[\mathbf{A}\,\mathbf{S}(k)\mathbf{S}(k)^H\,\mathbf{A}^H\right]. \tag{3.16}$$

Noting that we have already assumed that signal and noise are uncorrelated and that the array manifold matrix is a unitary matrix – since it has a Vandermonde form – we can express the covariance of the received signal as

$$\mathbf{R}_y = \mathbf{R}_s + \mathbf{R}_n = \mathbf{A}\,E\left[\mathbf{S}(k)\mathbf{S}(k)^H\right]\mathbf{A}^H + \sigma_\omega^2\mathbf{I}, \tag{3.17}$$

As per the definition in [22], the conventional beamformer has pre-calculated weights, independently from the incoming waves. In most cases, we consider the *weight matrix* to be the Hermitian of the array manifold matrix $\mathbf{w} = \mathbf{A}^H(\phi)$ (assuming the pre-established conditions at the beginning of this chapter). As explained earlier, we referred to the conventional beamformer using the time-domain signal model referred to previously in (3.6). For our concerned subject, we measure the maximum power in all directions around the array, power peaks are the estimated AoAs, according to

$$\mathbf{P}(\phi) = \frac{\mathbf{w}\,\mathbf{R}_y\,\mathbf{w}^H}{\mathbf{A}^H(\phi)\mathbf{A}(\phi)}, \tag{3.18}$$

where $\mathbf{R}_y$ is the received signal covariance as referred to in (3.17).

3.2.2 MUSIC

As stated before, algorithms for estimating DoA can be classified into beam-scan algorithms and subspace algorithms [22]. During our studies of various algorithms, we got to find out that the most prominent of these algorithms is the MUSIC algorithm. It is widely used because of its performance capability, and various versions and modifications of the MUSIC algorithm have been extensively studied. MUSIC is an eigenspace algorithm which utilizes the fact that each of the signal and the noise (assuming it to be AWGN) has a subspace that is orthogonal to the other [14].

From the EVD of the correlation matrix stated in (3.17), we order the resulting

eigenvalues in descending order. We assume that D (the number of sources) is known. We take the largest D eigenvalues as the ones representing the signal subspace. Thus, the ones $(N-D)$ left to be the ones representing the noise subspace. At this point, we have managed to move our problem to the subspace. The EVD is represented by

$$\mathbf{R}_r = \mathbf{Q}\Lambda_r\mathbf{Q}^{-1}, \tag{3.19}$$

where Λ_r is the matrix, whose diagonal contains the corresponding eigenvalues of concern and has the form

$$\Lambda_r = \begin{bmatrix} \lambda_1 & 0 & 0 & ... & 0 \\ 0 & \lambda_2 & ... & 0 & 0 \\ & & ... & & \\ 0 & ... & \lambda_D & ... & 0 \\ & & ... & & \\ 0 & 0 & 0 & ... & \lambda_N \end{bmatrix} \tag{3.20}$$

as $diag(\Lambda_r) = \lambda_1, \lambda_2, ..., \lambda_N$ are the eigenvalues of $\mathbf{R}_r$, and with prior knowledge of D, the eigenvalues of the correlation matrix are put in descending order from the first to the $(D+1)$th, yet between $(D+1)$th to (n)th eigenvalues are equal to each other $\lambda_1 > \lambda_2 > ... > \lambda_D > \lambda_{D+1} = \ ... = \lambda_N$. Meanwhile, $\mathbf{Q}$ is the matrix containing all eigenvectors of $\mathbf{R}_r$, whose vectors are put in order corresponding to the order of their eigenvalues, so that the eigen vector matrix takes the form

$$\mathbf{Q} = [\mathbf{q}_1 \ \ \mathbf{q}_2 \ \ ... \ \ \mathbf{q}_N], \tag{3.21}$$

Whenever the received waveform consists of D plane-wave signals plus uncorrelated noise, we could immediately reduce the problem from an N-dimensional problem to a D-dimensional problem. This reduction was accomplished, as long as D is known and less than or equal to $N/2$ so that it can define a signal subspace. Once the signal subspace was created, all further processing was done in that subspace [14].

Using the prior information that the noise is completely uncorrelated to the signal, we conclude that the steering vector in the subspace is orthogonal to the noise subspace. Therefore, multiplying the steering vector by the $(N-D)$ eigenvectors

will always be zero. We split the eigenvector matrix $\mathbf{Q}$ into signal subspace $\mathbf{Q}_s$ and noise subspace $\mathbf{Q}_n$ so that

$$\mathbf{Q} = [\mathbf{Q}_s \ \mathbf{Q}_n], \tag{3.22}$$

where

$$\mathbf{Q}_s = [\mathbf{q}_1 \ \mathbf{q}_2 \ \dots \ \mathbf{q}_D], \tag{3.23}$$

corresponding to the eigenvalues $\lambda_1, \lambda_2, ..., \lambda_D$,

and

$$\mathbf{Q}_n = [\mathbf{q}_{D+1} \ \mathbf{q}_{D+2} \ \dots \ \mathbf{q}_N], \tag{3.24}$$

corresponding to the eigenvalues corresponding to the eigenvalues $\lambda_{D+1}, \lambda_{D+2}, ..., \lambda_N$. Based on the orthogonality feature that we mentioned before the spatial spectrum of our array can be represented by

$$\mathbf{P}(\phi) = \frac{1}{\mathbf{A}^H(\phi)\mathbf{Q}_n\mathbf{Q}_n^H\mathbf{A}(\phi)}, \tag{3.25}$$

so that the peak values of $\mathbf{P}(\phi)$ correspond to the D angles of arrival that we are looking for.

MUSIC has been researched and a number of modifications have been made on it to enhance its performance, e.g. root MUSIC, beamspace MUSIC. We find no space to explain more about them in this report. For more detailed readings, we refer the reader to [13], [14] and [24].

3.2.3 Simulation results

To compare the performance of both algorithms explained above, several simulations were performed. Figures 3.3 and 3.4 show the results of simulations performed on a 5 element ULA (3.3) and a 5 element UCA (3.4). The simulations were done with 1000 samples and 15 dB SNR (Signal-to Noise Ration) for 20 and 50 degrees. As the figures show the difference in performance between conventional beamformer and MUSIC, MUSIC shows more precise angle estimation. The beamformer algorithm functions as long as the the number of sources does not exceed the number of antenna elements $D \leqslant N$ for ULA. However, the beamformer shows poor performance for UCA. MUSIC keeps performing well with UCA as long as the number of sources is known or it has been estimated correctly. In conclusion, MUSIC is more efficient than conventional beamformer under the conditions of suffiecient SNR and with knowledge of the number of sources D. Yet, the computational complexity of MUSIC is higher than

the beamformer. Practically, calculating the EVD of a relatively large matrix requires high processing resources, otherwise it can be time-consuming. There are – as previously stated – other options for algorithms that range between MUSIC and the beamformer in complexity and performance. The decision is to choose an algorithm that provides proper performance and require not-very high processing.

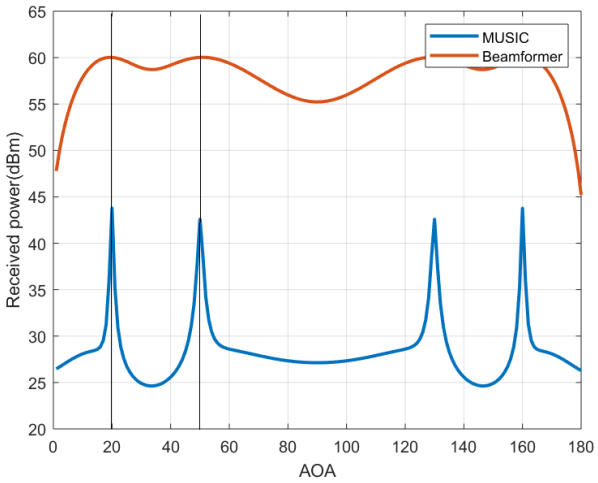

Figure 3.3: Simulation of beamformer versus MUSIC with a 5-element ULA.

3.3 Number of sources estimation

Some algorithms require knowledge of the number of sources to apply. MUSIC and other subspace algorithm are of this type, unlike beamspace algorithms that do not require this prior knowledge of the number of sources. The process to decide the number of sources differs in difficulty depending on the environment. An environment that causes none-to-low MPCs (Multipath Components) would result in mostly LOS beams. Hence the number of sources will directly be the number of plane-wave signals. If none of the signals are coherent with each other, the rank of the subspace equals the number of signals [14] (the author means that the eigenvalues of the noise subspace are very small, close to zero, so can be taken as zero). On the contrary, calculating the number of sources in an environment with reflectors can be tricky. Having a large number of MPCs meaning receiving many correlated signals. As stated earlier, the eigenvalues of the correlation matrix can be put in descending order from the first to the $(D+1)$th, yet between $(D+1)$th to (n)th eigenvalues are equal to each other $\lambda_1 > \lambda_2 > ... > \lambda_D > \lambda_{D+1} = ... = \lambda_N$.

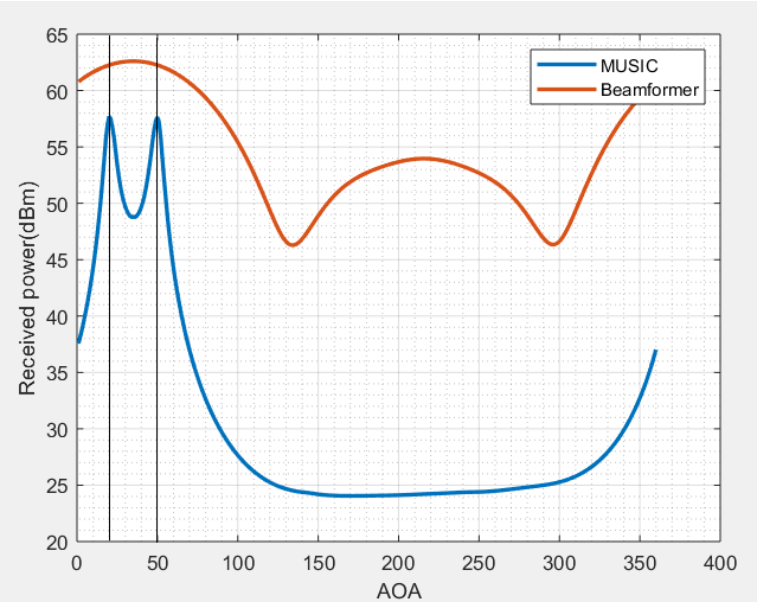

Figure 3.4: Simulation of beamformer versus MUSIC with a 5-element UCA.

Considering the case of uncorrelated sources, we would be able to see a large gap between the values of the largest D eigenvalues and the rest. As not only the smaller $(N-D)$ have -almost- equal values, but also they are significantly small. We can clearly see the gap between the values as in Figure 3.5. The simulation in the figure was done at $20, 50, 100$ degrees, SNR $=10dB$ and 1000 samples. In the case of coherent/correlated sources, there are different algorithms used for estimating the number of sources. However, this is out of the scope of this thesis. The reader can refer to [25] and [26].

3.4 Principal Error Sources

In any communication system, there are many sources that may cause an error, yet we can define the main sources so that they can be kept in an acceptable range. Principal Error Sources as defined by [27] are listed below:

- Receiver front-end noise

  Noise is a basic source of error in any communication system. Theoretically, we assume a reasonable Signal-to-Noise ratio (SNR) when simulating a system. However, practically, we can only control the *numerator i.e.* signal power. The system power budget is a key first step in any practical system implementation [27]. There are different ways to take in consider-

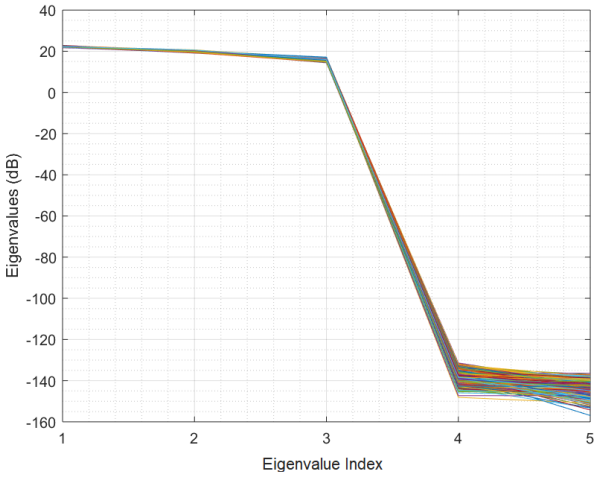

Figure 3.5: Eigenvalues of the signal-noise space ($D = 3$, $N = 5$).

ation when designing a system and there are different solutions for them. Yet, it is not the scope of this thesis [27].

- Signal waveform quantization

  What is meant here is the error resulting from Analog-to-Digital conversion (ADC), which is often similar to front end noise in terms of its effects on the received waveform [27]. It can take different forms depending on the modulation used and the type of variables being extracted (amplitude and angle or in-phase and quadrature samples,..). The bottom line is that ADC noise is very instrument-dependent. In other words, the more precise the hardware used is, the more this type of error can be reduced. Needless to mention that the quality of the hardware comes with a financial cost.

- Multipath components (MPC's)

  Multipath components are a major source of error in the majority of wireless systems. There are several algorithms to solve the multipath problem. Spatial smoothing is one of the most known algorithms. It is a mathematical solution for pre-processing the samples to solve this problem, which we briefly discuss here. Correlated sources result in a *non-full rank* correlation matrix. Thus, the problem appears. The advantage of spatial smoothing is that the correlation between the signals will be reduced [14].

  The author of [14] uses the frequency-domain snapshot model to define the

received signal spectral matrix

$$\mathbf{S}_x = \mathbf{V}\mathbf{S}_f\mathbf{V}^H + \sigma_\omega^2\mathbf{I}, \tag{3.26}$$

where $\mathbf{S}_f$ is the source signal spectral matrix and $\mathbf{V}$ is the steering matrix in the frequency domain.

Here, we take the case of a ULA. The antenna array is divided into L subarrays, each of length M elements.

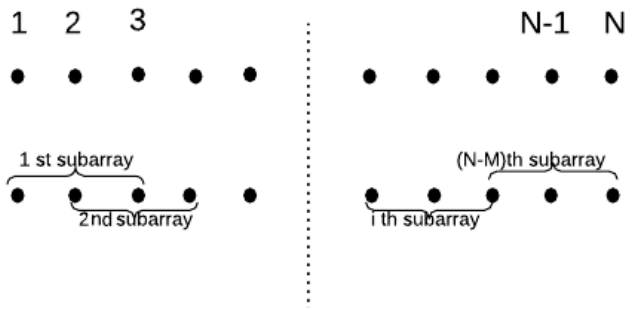

Figure 3.6: Spatial smoothing illustration.

A subarray i has a *forward* spectral matrix S_M^i and a *backward* one S_{MB}^i, which is a rotated form of the forward matrix

$$S_{MB}^i = J[S_M^i]^* j, \tag{3.27}$$

where J is a square exchange matrix of the relevant size taking the form

$$\begin{bmatrix} 0 & 0 & 0 & \dots & 1 \\ 0 & 0 & \dots & 1 & 0 \\ & \dots & & & \\ 1 & \dots & 0 & 0 & 0 \end{bmatrix}$$

A weighted average across all the subarrays is done, so that we can obtain a *smoothed* spectral matrix. For details and equations of the algorithm, the reader may refer to [14].

- Calibration/monitoring errors

  Practically, we need to place calibrating or monitoring devices when measuring the AoA of a source or using any other direction finding technique.

These electric /electronic devices cannot be avoided but still have an effect on the sensitive environment the measurements take place, and consequently on the system performance. Such impact must be considered in practice.

3.5 Lateration and angulation

Practically, one locator estimates one angle or one distance. In a 3-D scenario, this would mean a sphere (when estimating distance) or a circle (when estimating direction). Lateration and angulation use pre-determined information from the locators to estimate the location of an object.

In other literature, the terms ”trilateration” and ”triangulation” are used. The prefix “tri” means detection of the position requires 3 fixed points/angles at least. Lateration exploits ToA, TDoA and RSS measurements to detect the position of an object through finding the distance between the object and reference nodes using the geometry of space in a similar way as triangulation. This method (lateration) makes use of the point of intersection formed by three circles to determine the exact position, which is the method used in GPS systems. But, unlike triangulation which uses angle measurements. Angulation technique depends on direction finding information (AoA or AoD) measurements. Similarly, it uses triangle geometric properties to find the position of the sender [2], [28], [29], [30].

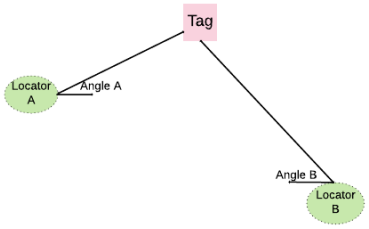

Figure 3.7: Angulation overview

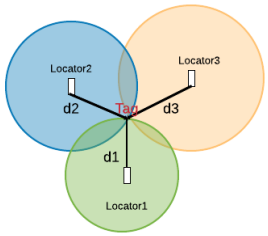

Figure 3.8: Lateration overview

3.6 Summary

In this chapter, a brief theoretical introduction about antenna array processing was given. Two examples of direction finding algorithms, as well as the main sources of error were discussed. In theory, algorithms such as the ones mentioned in this chapter can show very good results when simulated. However, in practice, they can be demanding when it comes to processing capabilities. Thereupon, manufacturers use simpler, less demanding algorithms when estimating AoA. To

reach acceptable accuracy, there are certain factors to be considered and scaled properly. As a conclusion, we can say that there is no standard antenna array geometry or direction finding algorithm which can be described to be the best for an indoor positioning system. Performance versus cost is the trade-off that appears when designing an IPS, whether it is regarding choosing an antenna array form or an estimation algorithm. In general, the performance of an indoor positioning system increases as long as the array geometry, direction finding algorithm and filtration are chosen carefully. The coming chapter analyses the system designed and manufactured by Texas Instrument (TI), which is the IPS that the practical part of this thesis is based on.

Chapter 4

System Architecture

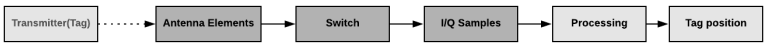

Figure 4.1: System Block Diagram.

In the previous chapter, a theoretical content was presented to open for the practical part that we base this thesis on. This chapter introduces the AoA BLE-based system that was put under test and evaluated. We start with a briefing about the history of Bluetooth. In the year 1989, a group of engineers, working for Ericsson (Lund, Sweden) designed and announced a new short-range communication technology that was named -years later -after the medieval Scandinavian king *Blåtann* in Danish, *Bluetooth* in English who united Denmark to be a single kingdom. The name was chosen to imply that Bluetooth ”unites” communication protocols. It was not until 1998, that Bluetooth Special Interest Group (SIG) was formed, and the name Bluetooth was officially adopted. The first Bluetooth specification ”Bluetooth V1.0” was released in 1999. Only a few years later, the newly-standardized communication system was common on hundreds of thousands of mobile phones, personal computers (PCs) around the world. In 2004, Bluetooth SIG adopted Core Specification Version 2.0 Enhanced Data Rate (EDR), at the time Bluetooth had been installed on 250 million devices. Bluetooth V4.1, including Bluetooth Low Energy (BLE) technology was launched in the 2010, opening the door for IoT. In January 2019, Bluetooth V5.1 was released with a new feature to support direction finding application [31], [32], [33].

With its revolutionary features, Bluetooth Low Energy has set a new standard for the technology. Now, Bluetooth can primarily be divided into Basic rate(BR)/EDR as one category versus BLE.

	BR/EDR	**BLE**
Frequency Band	2.4GHz ISM Band	2.4GHz ISM Band
Number of channels	79 (with 1 MHz spacing)	40 (with 2 MHz spacing)
Modulation	GFSK , $\pi/4$ DQPSK, 8-DPSK	GFSK
Power Consumption	1 (reference value)	0.01 - 0.5 of reference value
Data Rate	BR= 1 Mbps - EDR= 2, 3 Mbps	125, 500 kbps, 1, 2 Mbps

Table 4.1: Bluetooth BR/EDR versus Bluetooth LE
(Data source: [34])

4.1 BLE Background

BLE communication consists primarily of small packets of data called *"Advertisement packets"* broadcasted at regular intervals via radio waves by Beacons or other BLE enabled devices. It has 40 channels; three of them (Channel 37, 38, and 39) are used for broadcasting advertisement messages.

A quick summary of the main characteristics of Bluetooth can be quoted from [11]: *Bluetooth devices operate in the unlicensed 2.4 GHz ISM (Industrial Scientific Medical) band. A frequency hop transceiver is applied to combat interference and fading. Two modulation modes are defined. A mandatory mode, called Basic Rate, uses a shaped, binary FM modulation to minimize transceiver complexity. An optional mode, called Enhanced Data Rate, uses PSK modulation and has two variants: π /4-DQPSK and 8DPSK. The symbol rate for all modulation modes is 1 Msym/s. The gross air data rate is 1 Mb/s for Basic Rate, 2 Mb/s for Enhanced Data Rate using π /4-DQPSK and 3 Mb/s for Enhanced Data Rate using 8DPSK. A Time Division Duplex (TDD) scheme is used in both modes. This specification defines the requirements for a Bluetooth radio for the Basic Rate and Enhanced Data Rate modes.*

Basically BLE5.1 has been enhanced with the extension added to the standard BLE packet as found in BLE4.2. In Figure 4.2, we can see that the constant

tone extension (CTE) is added *after* the CRC part in the packet. Previously, the BLE packet ended by the CRC part. The constant tone extension is a section of consecutive 1's without whitening, which is effectively a +250kHz wave on top of the carrier wave. In the Bluetooth Core Specification V5.1, both periodic advertising packets and connection packets can contain a constant tone extension after the CRC. The CTE can only be sent using uncoded PHY [35]. As shown in Figures 4.2) and (4.3, we can see the fundamental difference between an uncoded PHY BLE packet and a coded PHY one.

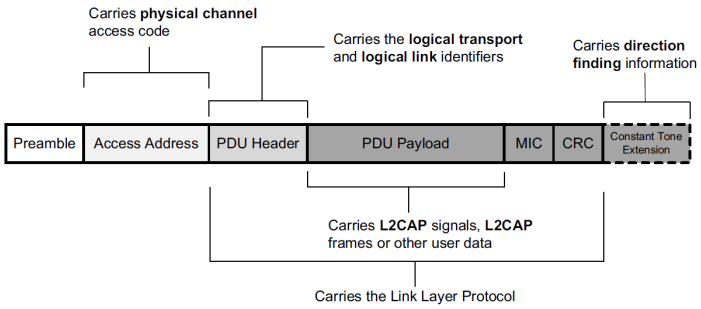

Figure 4.2: The packet structure for the BLE Uncoded PHY [11].

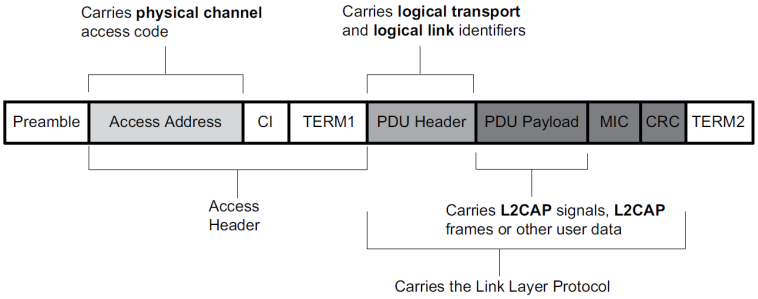

Figure 4.3: The packet structure for the BLE Coded PHY [11].

An LE device can make its direction available for a peer device by transmitting direction finding enabled packets. Using direction information from several transmitters and profile-level information giving their locations, an LE radio can calculate its own position. The peer device, consisting of an RF switch and an antenna array, switches antennae while receiving part of those packets and captures IQ samples. The IQ samples can be used to calculate the phase difference in the radio signal received using different elements of the antenna array, which in turn can be used to estimate the angle of arrival (AoA) [11].

4.2 TI system physical layer

4.2.1 System architecture overview

The physical layer of the IPS in the locator (receiver) consists of an antenna array board. Geometry, antenna type and spacing between antennas are the main parameters in each array configuration, different array configurations have different effect on the received data.

In theory, we could say that the larger number of antenna elements and the more complex the geometry is, the better and more accurate the resulting angle would be. However, this does not come with no cost. Practically, manufacturers usually choose to have simple antenna geometry and relatively few number of elements due to cost concerns. In our project, we have worked with Texas Instruments (TI), providing two of their products which together form the AoA estimation system:

1. The first product is the CC2640R2 LaunchPad: a battery-powered device equipped with transmitting/receiving antenna operating at Bluetooth frequency 2.44 GHz. Device specifications can be found at [36].
2. The second product is BOOSTXL-AOA antenna array:a externally-powered board. Device specifications can be found at [37].

TI suggested two ways for the system set-up:

- In the first one, we have a sender (transmitter/signal source) LaunchPad. And a BOOSTXL-AOA plugged to a second LaunchPad, the later two work together as a receiver/locator, as illustrated in Figure 4.4.
- The second suggested module combines one BOOSTXL-AOA board plus 3 LaunchPads. One LaunchPad plugged to BOOSTXL-AOA board (a passive unit), in addition a second LaunchPad (a master unit), both the master and the passive communicate together through a node manager (a PC). All together form the receiver. On the other side, we have one LaunchPad to locate (slave/transmitter), illustrated in Figure 4.5.

For simplicity we would refer to the first module “AOA module” (1 BOOSTXL-AOA + 2 CC2640R2 LaunchPads) as “Module 1”. The second module “RTLS module” (1 BOOSTXL-AOA + 3 CC2640R2 LaunchPads) as “Module 2”. We have to emphasize that both use similar algorithms and do the same function – which is to estimate the angle of arrival. We compare the performance of both to discuss the effect of adding an extra processor unit (*i.e.* doubling the processing power).

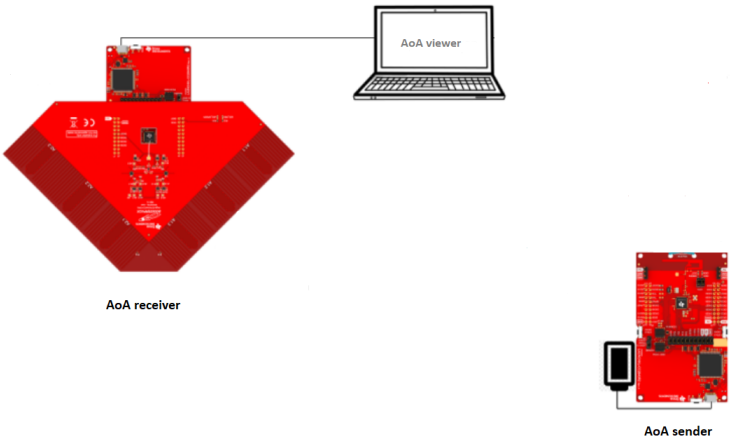

Figure 4.4: Module1 representation.

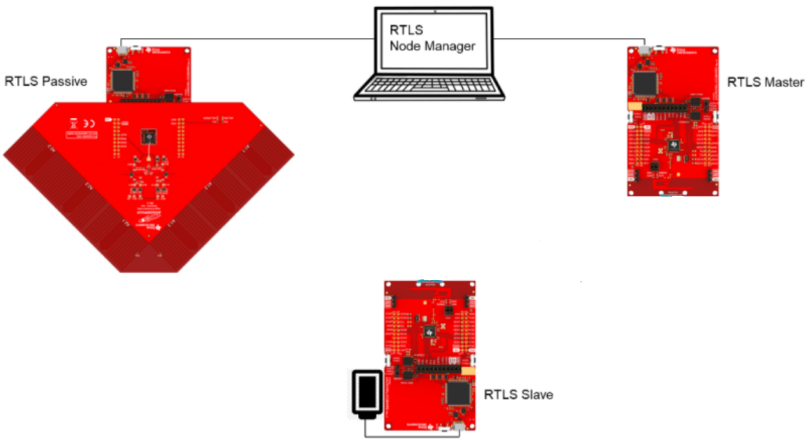

Figure 4.5: Module2 representation.

4.2.2 Antenna Array BOOSTXL-AOA

Our antenna array in reality consists of two ULAs perpendicular to each other, each has 3 dipole antenna elements. Each side of the board reads data separately, calculates an AoA and after calculating one angle from each side, the locator chooses the angle from the array with the higher RSS.

As stated in the previous chapter, ULA has ambiguity in the AoA estimation, as the array can not decide which side is the signal coming from, *i.e.* on a 360 degrees, a ULA can not differentiate between ϕ and $(2\pi - \phi)$. This problem could be overcome by having 2 perpendicular ULAs forming a triangle. Metal grounding on the board on both sides of all antenna elements help "attenuate" receiving signal from behind the ULA, allowing signal from the front side of each ULA to have much higher RSS in comparison. As we come later in the next section, the system chooses the AoA estimation done by the ULA that receives signal with the higher RSSI. Consequently, the two ULAs will still estimate angles between 0 - 180 degrees, but we would be more certain about which side the signal comes from, because of the power difference between the two arrays, *i.e.* the first ULA (on the left) would estimate angles between 0 - 90 degrees and the second ULA (on the right) as appears in Figure 4.6. In addition, the 2 ULAs are geometrically orthogonal and therefore, they have orthogonal polarization. Hence, the ambiguity problem is solved without the need for using an UCA.

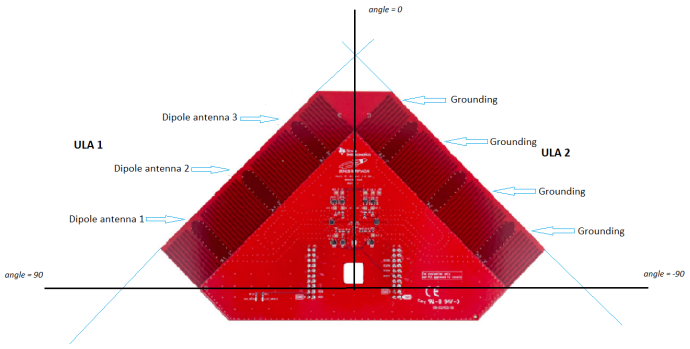

Figure 4.6: BOOSTXL-AOA antenna array board.

4.3 System algorithm overview

The signal source transmits an advertising packet. The structure of this packet is known, and it includes a continuous signal which simplify the analysis. The receiver get this packet and starts switching between each element in the array.

Each element reads and records IQ samples within a pre-defined time slot. The signal at each element is a delayed version of original signal, this delay appears as a phase shift. Combining each antenna output in a smart way at a given time instant we can get an N-dimensional observation vector as an array output. Based on the observation vectors and algorithm, the location of the transmitter can be calculated [13], [38]. When processing antenna arrays in theory, the sampling is considered to done at all antenna elements in the same time. In practice, that would require a massive processing capability to operate N receivers simultaneously. As mentioned, samples are taken from elements periodically. We assume that neither the locator or the source are in motion and the environment is stationary. So that, an RF switch is toggled periodically between the elements to take samples. After it is done with one array, another switch flips to the other ULA to do the same thing.

From the schematic of the array in Figure 4.7, it is shown that each antenna array is connected to an SP3T RF switch. As well as, an SPDT RF switch between the two arrays. The reader can find device specifications in [39] and [40]. The output of the SPDT RF switch is connected through an JSC connector for the analog output to the LaunchPad. Yet, the whole BOOSTXL-AOA board is connected to LaunchPad with 2 JTAG connectors for power supply and digital AND gate control. For more details about the BoosterPack, please refer to the manufacturer website [37].

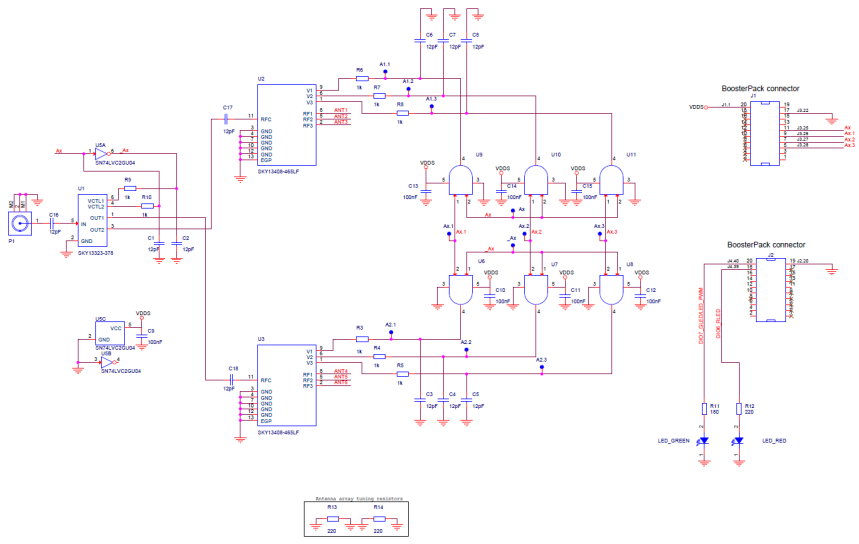

Figure 4.7: BOOSTXL-AOA Schematic [41].

Using a special RF Core patch in receive mode, the I and Q samples from the transmitted carrier frequency + 250kHz tone can be captured, pre-processed, and buffered by the RF Core without any load on the main micro-controller unit (MCU). The IQ samples can be captured at a rate of up to 4 MHz and a resolution of 16 bits (32 bits per I/Q data pair) $\rightarrow$ 128 *bits*/μs $\rightarrow$ *1kB holds* 64 μs and the buffer size can be up to 2kB (128μs of 4MS/s data). The RF Core can provide control signals directly to the antenna switches through CC2640's IOs, and divides the total capture period into slices for each antenna. The slice length (or antenna dwell time) will determine the accuracy of the phase measurement (default 4μs) [42], [43].

Due to the design of the antenna board, there is indeed a phase difference between the antennas. So we extract the phase difference between `ant1_sample` [8 to 15] and `ant2_samples` [8 to 15], where `ant1_sample` and `ant2_samples` are the IQ samples in antenna number 1 and antenna number 2 respectively, each containing 16 samples. The switch among antennas will cause measurement error, therefore we discard I/Q samples from 0 to 7 when calculating angles [42]. After sampling and during the post processing, the first 8 samples of each 16 are discarded as they are taken during the switching and antenna settling time. Therefore, they can be undependable.

The phase difference between 2 IQ samples (Φ) is calculated according the below

$$
\begin{aligned}
IQsample_1 &= a_1 + jb_1 \\
IQsample_2 &= a_2 + jb_2 \\
Z &= IQsample_1.(IQsample_2)^* \\
&= a_1a_2 + b_1b_2 + j(a_2b_1 - a_1b_2) \\
\Phi &= \tan^{-1}(\frac{Im(Z)}{Re(Z)})
\end{aligned}
$$

Afterwards, the phase difference is calculated between antenna pairs for each ULA. In other words, the three elements of each ULA form three pairs and the three phase differences resulting formulate the basic estimated AoA. It is taken into consideration that the phase difference between the first and third antennas is double what it is between the first and the second or the second and the third. The phase difference is averaged over a block of data of 512 IQ samples. While calculating the phase difference between the antenna elements, the phase drift that may be caused by frequency inconsistency is added to make sure the phase difference represents the desired angle.

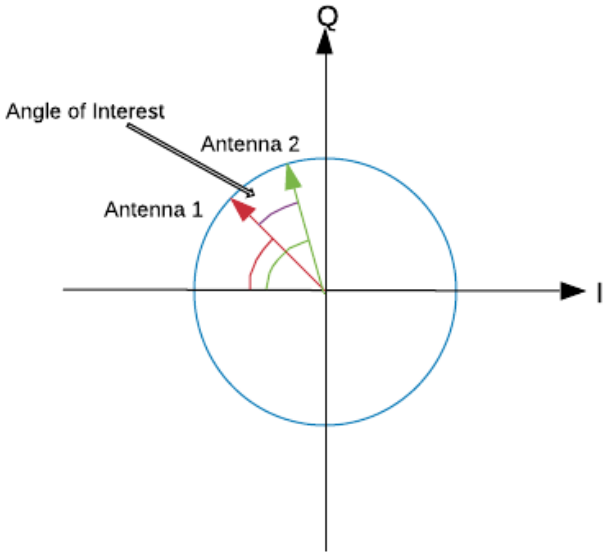

Figure 4.8: Phase difference between 2 IQ samples.

An important factor to bring into attention is the difference in channel frequencies and consequently, wavelengths. The differences in the wavelengths shall result in a drift in the calculation, as all antennas and system design is in reference to the center frequency f_c = 2440 MHz of wavelength λ_c = 12.3 cm. Due to that, the manufacturer suggests adding a *channel offset*. Table 4.2 compares the channel frequencies, wavelengths and the correction suggested by TI to fix the drift.

Channel number	Frequency(MHz)	Wavelength(cm)	Angle correction (degrees)
37	2404	12.49	-10
38	2426	12.37	-5
39	2480	12.1	15

Table 4.2: Bluetooth channel corrections.

In addition to that, there are other factors that may cause a drift in the calculations. Antenna beam pattern imperfection, separating distance and the surrounding environment can cause a deviation that is suggested to be corrected by a gain and an

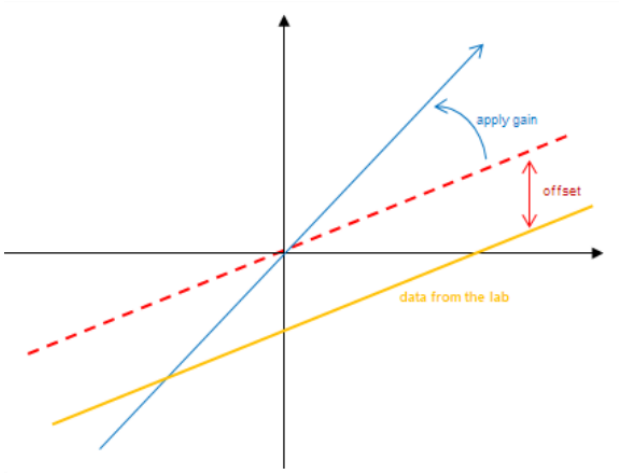

Figure 4.9: System offset and gain alteration [43].

offset. TI suggests a correction factor between pairs that needs to be calibrated for different environments. The measurements done in the next chapter were all done with the same antenna correction factors even though they were taken in different environments for the sake of comparison.

4.4 Summary

Different aspects of our TI IPS were illustrated in this chapter. A BLE background and specifications, demonstration of the physical layer of the system, and the factors added to enhance its estimation methodology. In the next chapter, the results of the measurements done on the IPS are discussed and compared with the expectations provided by the manufacturer and driven from prior theoretical studies as illustrated previously in Chapter 3.

Chapter 5

Empirical Measurements

Our expectation for the system performance was to have an accuracy of +/-4 degrees in an anechoic chamber [37]. In order to evaluate the system performance, several tests have been conducted. During our measurements, we chose different environments and applied different testing scenarios. We have kept the main criteria such as distance between transmitter and receiver, transmitted power and target angles the same. With a separating distance of 160 *cm* between the centre of the antenna array and the transmitting antenna, measurements were done through the angles from -90 to 90 degrees in steps of 15 degrees in the below different environments:

- anechoic chamber, shown in Figure 5.1.
- long corridor (width=2m), shown in Figure 5.2.
- sports hall ($15.5x10.5x3m$), shown in Figure 5.3 and Figure 5.5.
- meeting room($8x5x2.7m$), shown in Figure 5.4 and Figure 5.6.

In this report, we represent the results using **"Box Plots"** as they can visually represent the data in a sufficient way showing the median of the samples and how variant the samples are. The name "box" comes from plotting the samples between 25th and 75th percentile in the box with the median of the samples represented by a red line in the middle. As shown in Figure 5.7, the outlier values are represented by the red small crosses and *adjacent values* by the black lines above and below the box. The reader can refer to [44] and [45] for more details about Box Plot representation.

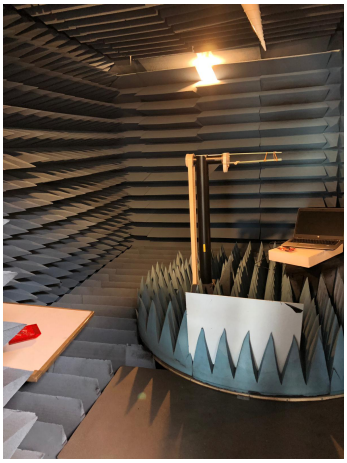

Figure 5.1: Anechoic chamber.

Figure 5.2: Corridor.

Figure 5.3: Sports hall.

Figure 5.4: Meeting room.

5.1 Anechoic chamber measurements

Figures 5.8 and 5.9 show the box plot representation of the measurements. As we notice that the *blue boxes* on the plots are relatively small, meaning that the readings were stable around the median value most of the time. The outliers are not very spread out, yet noticeable. It is crucial to mention here that it was unavoidable to have measuring equipments (laptops, USB cables,..) in the anechoic chamber to be able to save the readings, which could justify the outlier values due to reflections or interferers cause by the extra equipments. Yet, plotting the mean angle error for both modules 1 and 2 - defined as the difference between the mean measured values and the actual values - we can see that the *suggested* error margin by the manufacturer was broken as appears in Figure 5.10.

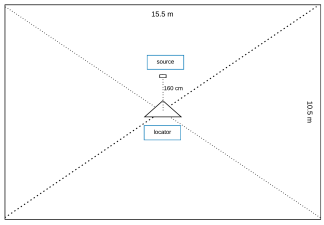

Figure 5.5: Sports hall schematic.

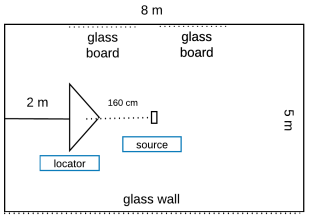

Figure 5.6: Meeting room schematic.

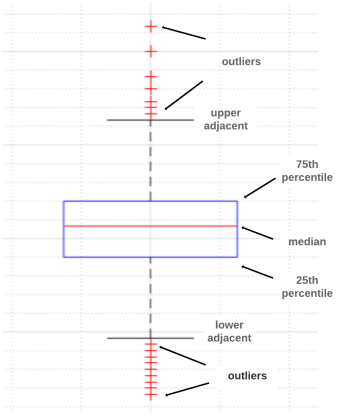

Figure 5.7: Box plot overview.

5.2 Module1 versus Module2

Comparing the results for the measured angles in the anechoic chamber as shown in Figures 4.4 and 4.5 for modules (Module1 & Module2) – in subsection 4.2.1 – under the same circumstances, we see that the mean angle error is close for most angles. Meaning that the mean angles are close under the same period of time. Yet, there are more outliers in case of Module1. Here, we have to keep in mind that the number of AoA results of Module1 were almost 4 times as many as the results of Module2 per angle. A reason that the outliers are more spread in Module1 is that they were more likely to happen due to the larger number of samples compared to Module2. The difference between the upper and lower adjacents is what we are most considered of. As appears in the figures, the adjacents are narrower in Module1, despite the larger number of samples.

In the other scenario, measurements in the meeting room represented in Figures 5.12 and 5.13 shows more outliers in Module1 than Module2. Additionally, it shows a higher variance in Module2 than Module1 as the lower and upper ad-

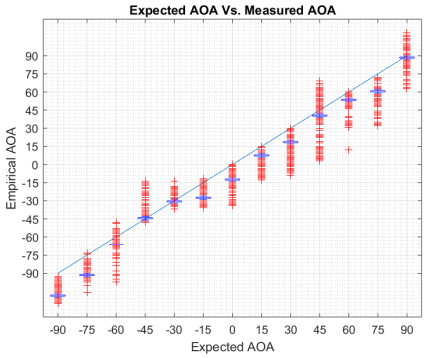

Figure 5.8: Module1-anechoic chamber.

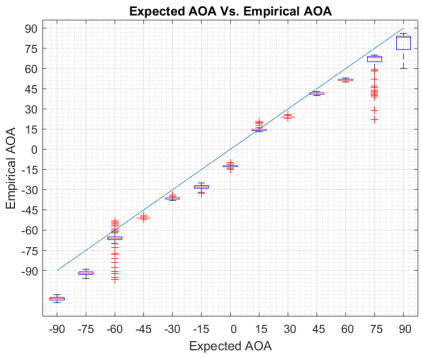

Figure 5.9: Module2-anechoic chamber.

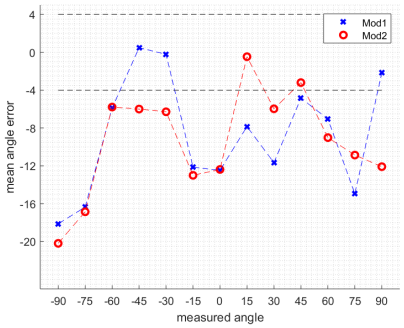

Figure 5.10: Mean angle error in anechoic chamber.

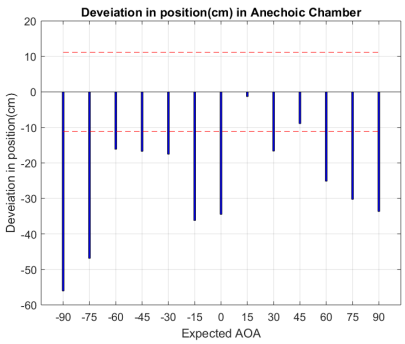

Figure 5.11: Estimated error in distance.

jacents are much more spread in Module2 (even if Module2 has fewer outliers). The mean error angles in Figure 5.14 turn to increase on both edges and for both modules but at narrow angles (between -30:30 degrees), Module1 shows better performance. The meeting room – where the measurements were taken – was not an ideal environment per se. Still, the performance of Module2 was not much better, which leads us to the conclusion that increasing the processing resources has not resulted in the expected enhancement in estimating the angle of arrival.

As mentioned above, regarding the gap between the number of AoA results for both modules. As well, from the structure of the two modules – check Figures 4.4 and 4.5 – we can see that the structure of Module2 contains 3 units altogether forming the locator (RTLS master, RTLS passive and RTLS node manager) the processing and communication between the three elements to estimate one AoA result took almost *quadruple* the time when the processing is done only on one element. Longer processing time for Module2 caused that under the same period and circumstances, we got a fewer number of AoA per minute compared with

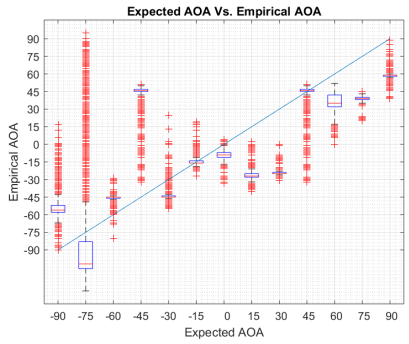

Figure 5.12: Module1: meeting room.

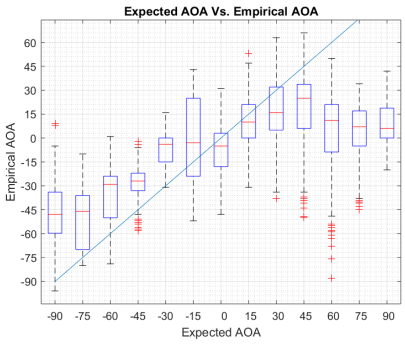

Figure 5.13: Module2: meeting room.

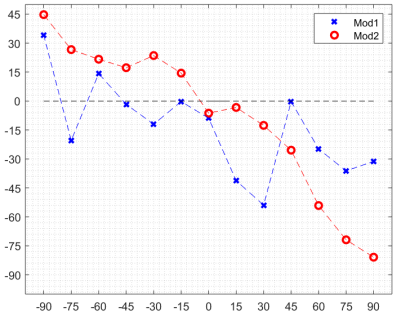

Figure 5.14: Mean error comparison: meeting room.

Module1. Here, we can say that the system reaches its maximum capabilities with one LaunchPad acting as a locator. In other words, splitting the locator function between two LauncPads means only extra financial cost with no enhancement in the results.

5.3 Effect of environment

The accuracy of AoA estimation depends on the environment where it takes place. The geometry of the room/area and the surrounding material and objects determine altogether how the signal components behave. The four environments where measurements were taken – check Figures 5.1 to 5.6 – differ drastically. Below we discuss how these differences affect the AoA measurements.

Comparing Figure 5.8 of the anechoic chamber measurements with Figure 5.16 of the corridor measurements, the measurements done in the corridor showed very poor results (45 degrees of error in some cases). The mean angle error deviated from some angles to others due to the geometry of the corridor and the place-

ment of both the transmitter and the receiver. On top of that, there were metal doors and metal pipes attached to the ceiling. These surroundings were chosen to test the system under ”severe” conditions. The metal parts acted as strong reflectors causing strong NLOSs. As well, the narrow corridor (width of almost 2 meters), helped the reflections to keep most of the power as they travel for a short distance.

In contrast, measurements performed in the sports hall, as shown in Figure 5.15, illustrate that the estimated median angles were much closer to the ones in Figure 5.8. In addition, how variant the samples are around the median are. The sports hall was a close-to-ideal environment. The size of the sports hall allows a clear LOS at all times and makes most reflection (NLOS components) travel for longer distances and time before reaching the locator. Consequently, NLOS components have relatively low RSSI. Consequently, they would not disturb the estimation on a significant scale. The material of the walls and the floor (that is mostly wood) helped a lot absorbing a large percentage of the reflected signal power. Therefore, NLOS MPCs have lower power than the receiver sensitivity and can not be read.

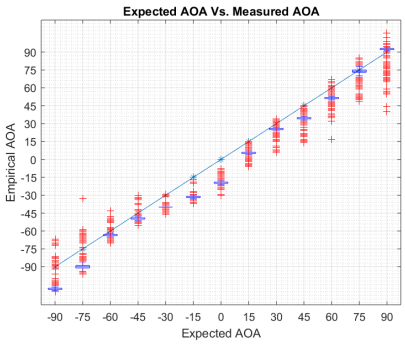

Figure 5.15: Module1: sports hall.

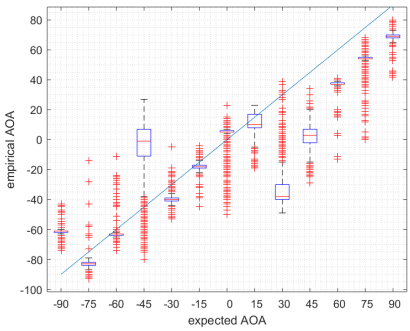

Figure 5.16: Module1: corridor.

Measurements in the meeting room, as shown in Figure 5.12, were similarly subject to the placement, geometry, wall material, and surrounding objects as well. This is clearly represented in the large variance in the results. Despite that the mean angle error was reasonable, a significant number of the angles were quite far from the median, positively and negatively. The room had a glass wall on one side, 2 glass boards on the opposite wall as was shown in Figure 5.6. That is why some angles were affected more than others with NLOS reflections. The wall acts as a reflector and helped the reflecting waves to keep most of their power resulting in strong NLOS, *i.e.* a poor estimation of AoA.

For a chosen angle of 45 degrees, we compare the results of Module1 in all the en-

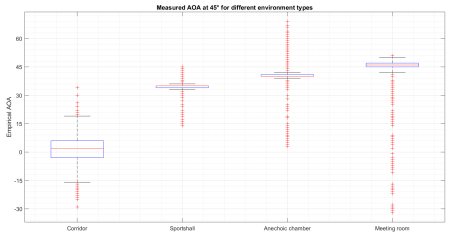

Figure 5.17: Module1: Different environments at 45 degrees.

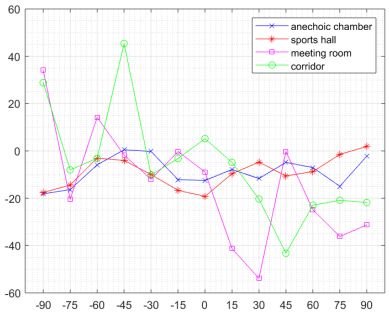

Figure 5.18: Module1: Mean angle error in different environments.

vironments. We can see that the worst estimated median AoA was the estimation -unsurprisingly- in the corridor. Not only that the mean of the angles was almost 45 degrees off the right angle, but also the variations in the reading were massive. The box of the $25th$ and $75th$ percentile is narrowest in both the anechoic chamber and the sports hall. Followed by the meeting room. Lastly, comes the corridor estimation. The median of the sports hall is yet slightly far from the precise estimation compared to the anechoic chamber. The median of the meeting room is the closest to 45, despite the fluctuation in 50% of the samples lying between the 25th and 75th percentile. As mentioned before, we are most concerned with the stability of the estimation, rather than the accuracy of the median.

Figure 5.18 – showing all measured mean errors versus angle – summarizes the stated above that regarding the effect of the environment. Furthermore, the figure shows what we can call an *"error pattern"*. Certain angles are more affected than others. It is more obvious for the anechoic chamber and the sports hall – since both have a uniform environment – that the error is minimal around both angles -45 and 45. The error slightly increases towards the center line of the board (angle 0) from both sides. The closer the angle measured to the edges of the board (closer to -90 and 90), the higher error it shows. This can be explained by the antenna beam pattern effect.

5.4 Antenna beam patterns

According to the manufacturer's support page [46]: *The dipole antennas are made shorter on purpose so that they can be placed closer together and with this, you sacrifice around 10 dB in efficiency. The exact resonance frequency is 2.44 GHz.*

Although the dimensions of the antennas are not half-wavelength ($6.15cm$) as expected, the board is designed to include layering, insulation, and grounding between the elements so that all elements resonate at $2.44GHz$. The ideal beam pattern of a dipole antenna is the famous doughnut shape. Yet, practically when measuring the beam pattern of the antennas, we find that the doughnut shape does not apply as it looks theoretically. Since the dipole antennas of the doughnut-shaped beam pattern are single polarized, we would expect that certain angles - in relative to the board, *i.e.* the angle being measured - would suffer lower gain than others. In addition, knowing that the antennas are single-polarized, the elevation angle still affects the gain.

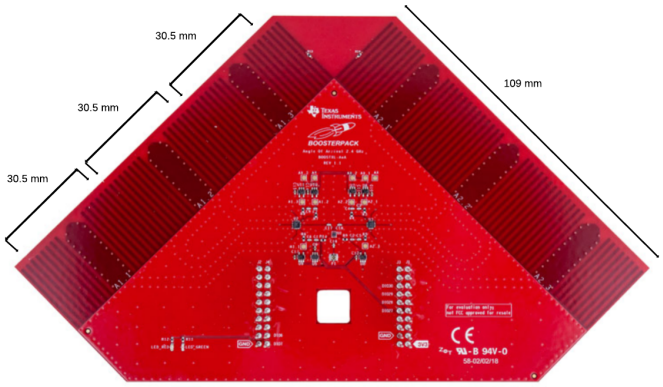

Figure 5.19: BOOSTXL-AOA board dimensions.

In the previous chapter, we have explained how the estimation of AoA is calculated by averaging the AoA between an antenna pair at a time. Non-identical beam patterns would result in a deviation from the real angle. The differences in antenna beam patterns between different elements are primarily caused by their placement on the board. In order to realize the differences between the beam patterns in the far field, we measured the beam patterns of one pair in the anechoic chamber. The measurements were taken for each antenna separately. So that, each time we keep one antenna active and all others on the board inactive.

Here, we have the first pair on the first array as an example. Figures 5.20 to 5.25 compare the beam patterns of the pair from different planes and polarizations where we notice how they vary in certain angle ranges. Figures 5.20 and 5.21 show the most obvious gap between the two patterns is very close to angle 90, which explains the error happening when estimating angles around that. In contrast, the patterns have almost the same gain at angle 45. At angle 0, there is a difference in the gain but much smaller than the one at angle 90. Plane $\phi = 0$ matches the plane that the measurements we have taken, *i.e.* elevation angle $\theta =$

0 and with the center line of the board matches $\phi = 0$. That is plane $\phi = 0$ beam patterns are the ones we are considered of the most.

Considering Figures 5.20 to 5.23, we can vaguely say that they look similar to the theoretical peanut shape for the beam patter of a dipole antenna. From these figures, we can expect the loss to be in a range of 10 – 15 dB. In addition, empirical measurements showed that the RSS for 45 degrees was about 7 dB above the RSS for 135 degrees. We keep in mind that the manufacturer suggested using the system between $[-128 : 128]$ degrees – for that reason – even though, that the array could measure in the range $[-135 : 135]$ degrees. The received power – even in case affected by the non-ideal beam patterns – would still be higher than the receiver sensitivity level (-93 dBm as per the manufacturer) at all times. Thus, we conclude that even using non-ideal, somewhat "commercial" dipole antennas can give the benefit of saving cost and does not affect the performance of the system as much.

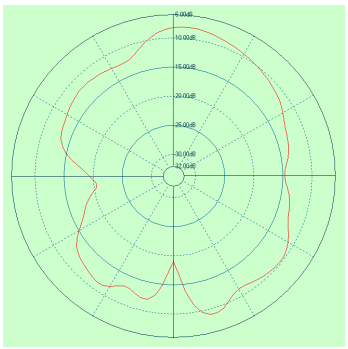

Figure 5.20: Antenna A1.1-plane $\phi = 0$.

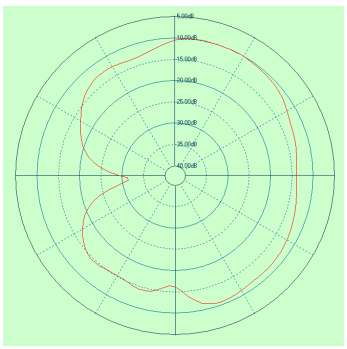

Figure 5.21: Antenna A1.2 -plane $\phi = 0$.

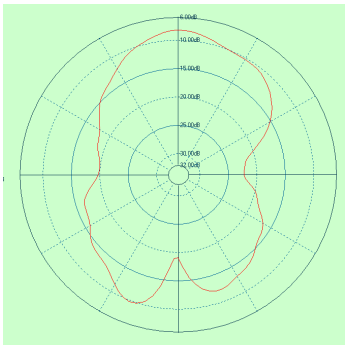

Figure 5.22: Antenna A1.1-plane $\phi = 90$.

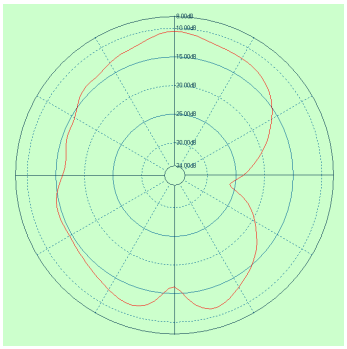

Figure 5.23: Antenna A1.2-plane $\phi = 90$.

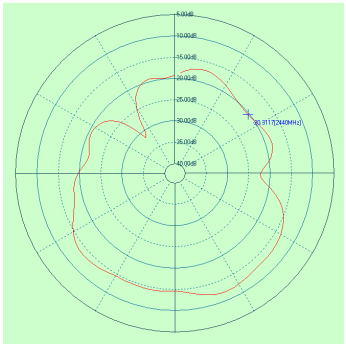

Figure 5.24: Antenna A1.1-plane $\theta = 90$.

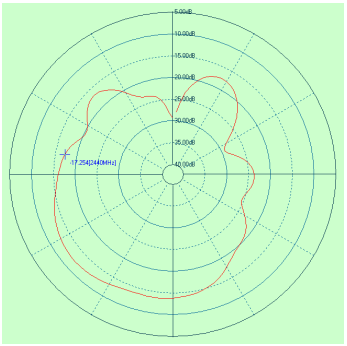

Figure 5.25: Antenna A1.2-plane $\theta = 90$.

5.5 Summary

This chapter exhibited the measurements done on both system modules, in different environments and compared the results from different aspects and drove findings with justifications. The next chapter discusses some conclusions and suggestions to keep in mind for future work.

Chapter 6

Conclusion

In this thesis, we have compared different technologies (GNSS, UWB, Bluetooth, and others) and from the pros and cons of each, we have found a sweet spot between complexity, accuracy, availability, and cost to be a Bluetooth-based IPS. As well, we have explored different techniques to be used with BLE (ToA, RSS and AoA) and chosen AoA as the most convenient due to the same reasons stated. The theoretical background of antenna array processing along with different algorithms have been discussed. Several experimental tests have been done with the aim to analyse accuracy level in Bluetooth AoA-based indoor positioning system using a commercial non-complex IPS system.

This work shows there is room for improvement. The results indicate the importance of LOS signal for IPS system, the multipath components caused by different environments objects affect the accuracy level. We have a few suggestions that we have concluded for future work to enhance the system performance:

- Switching between antenna elements can be enhanced. As stated in Chapter 4, 50% of the IQ samples read and saved are thrown away. Instead, it can be done smartly to reduce RAM and processing power. Different options can be introduced. Dynamic switching time between elements, depending on the environment. As well, a settling time window could be added in between the switchings, where no data is saved.

- Using a correlation reduction algorithm for the IQ samples read from the antennas can be beneficial – if combined with a carefully-chosen direction finding algorithm – so that reducing correlation would help lower the effect of the NLOS and consequently give a better AoA estimation.

- Capturing samples can be enhanced so that the array could read from two

(or more) antennas simultaneously which could give a better accuracy if the environment is not static enough. However, this would require several receiver chains, which would add extra cost.

- Antenna array design can be enhanced, whether by adding additional elements or changing the antenna array.

- The differences in the element beam patterns should be taken into account. Some post-processing calculations need to be done when the AoA is expected or initially evaluated at certain angles. The offset and gain of the phase suggested by the manufacturer can be adjusted depending on the expected direction of the source, or when not available, the initial calculation of the angle.

Future work continuing this thesis is to include the points suggested. The next step is testing and simulating these suggestions to have more insights. Such tests and simulation could help investigate the effect on the performance, in terms of accuracy, handling time, processing power, *etc*.

Bibliography

[1] P. A. Zandbergen, "Accuracy of iPhone locations: A comparison of assisted GPS, WiFi and cellular positioning," *Transactions in GIS*, vol. 13, pp. 5–25, 2009.

[2] S. Sadowski and P. Spachos, "RSSI-based indoor localization with the internet of things," *IEEE Access*, vol. 6, pp.30149–30161, 2018.

[3] H. Liu, H. Darabi, P. Banerjee and J. Liu, "Survey of wireless indoor positioning techniques and systems," *IEEE Transactions on Systems, Man, and Cybernetics, Part C (Applications and Reviews)*, vol. 37, no. 6, pp. 1067–1080, 2007.

[4] F. Zafari, A. Gkelias and K. K. Leung, "A survey of indoor localization systems and technologies," *IEEE Communications Surveys & Tutorials*, 2019.

[5] Y. Chen, "Evaluating Off-the-shelf Hardware for Indoor Positioning," M.S. thesis, Faculty of Eng., LTH, Lund Univ., Lund,2017. [Online]. Available: `https://lup.lub.lu.se/student-papers/search/publication/8905887`

[6] Pozyx online store. [Online]. Available: `https://www.pozyx.io/shop`

[7] Sewio UWB kit. [Online]. Available: `https://www.sewio.net/product/indoor-tracking-rtls-uwb-kit`

[8] A. Lindemann, B. Schnor, J. Sohre and P. Vogel, "Indoor Positioning: A Comparison of WiFi and Bluetooth Low Energy for Region Monitoring," *HEALTHINF*, 2016, pp. 314–321.

[9] M. Rouse, *CSMA/CA (Carrier Sense Multiple Access/Collision Avoidance)*, [Online]. Available: `https://searchnetworking.techtarget.com/definition/CSMA-CA`

[10] R. Mautz, "Indoor positioning technologies," Habilitation thesis, Institute of Geodesy and Photogrammetry, ETH Zurich, Zurich, 2012. [Online].

Available:
https://www.research-collection.ethz.ch/handle/20.500.11850/54888

[11] Bluetooth SIG, "Bluetooth Core Sprecification v. 5.1," Jan. 2019.

[12] A. F. Molisch, *Wireless communications*, John Wiley & Sons, 2012.

[13] F. Belloni, "Signal processing for arbitrary sensor array configurations: theory and algorithms," Ph.D. disseration, Helsinki University of Tech., Aalto Univ., Helsinki, 2007. [Online]. Available:
https://aaltodoc.aalto.fi/handle/123456789/2923

[14] H. L. Van Tress, *Optimum array processing: Part IV of detection, estimation, and modulation theory*, John Wiley & Sons, 2004.

[15] S. A. Schelkunoff, "A mathematical theory of linear arrays," *The Bell System Technical Journal*, vol. 22, no. 1, pp. 80–107, 1943.

[16] S. Haykin, *Advances in spectrum analysis and array processing (vol. III)*, Prentice-Hall, Inc., 1995.

[17] C. P. Mathews and M. D. Zoltowski, "Eigenstructure techniques for 2-D angle estimation with uniform circular arrays," *IEEE Transactions on signal processing*, vol. 42, no. 9, pp. 2395–2407, 1994.

[18] M. Al-Sadoon, N. Ali, Y. Dama, A. Zuid, S. Jones, R. Abd-Alhameed and J. Noras, "A new low complexity angle of arrival algorithm for 1D and 2D direction estimation in MIMO smart antenna systems," *Sensors*, vol. 17, no. 11, pp. 2631, 2017.

[19] P. Ioannides and C. A. Balanis, "Uniform circular arrays for smart antennas," *IEEE Antennas and propagation magazine*, vol. 47, no. 4, pp. 192–206, 2005.

[20] D. E. Davies and A. Rudge, "The handbook of antenna design," *London: Peregrinus*, vol. 2, 1983.

[21] P. Gupta and S. P. Kar, "MUSIC and improved MUSIC algorithm to estimate direction of arrival," *2015 International Conference on Communications and Signal Processing (ICCSP)*, pp. 757–761.

[22] V.Krishnaveni, T.Kesavamurthy and B. Aparna, "Beamforming for direction-of-arrival (DOA) estimation-A survey," *International Journal of Computer Applications*, vol. 61, no. 11, 2013.

[23] B. D. Van Veen and K. M. Buckley, "Beamforming: A versatile approach to spatial filtering," *IEEE assp magazine*, vol. 5, no. 2, pp. 4–24, 1988.

[24] A. Vesa, "Direction of arrival estimation using MUSIC and root–MUSIC algorithm," *18th Telecommunications Forum, Pg*, 2010, pp. 582–585.

[25] G. Xu, R. H. Roy and T. Kailath, "Detection of number of sources via exploitation of centro-symmetry property," in *1992 IEEE International Conference on Acoustics, Speech, and Signal Processing (ICASSP-92)*, pp. 349–352.

[26] G. Xu, R. H. Roy and T. Kailath, "Detection of number of sources via exploitation of centro-symmetry property," *IEEE Transactions on Signal processing*, vol. 42, no. 1, pp. 102–112, 1994.

[27] J. E. Evans, D. F. Sun and J. R. Johnson, "Application of Advanced Signal Processing Techniques to Angle of Arrival Estimation in ATC Navigation and Surveillance Systems," Massachusetts Inst of Tech Lexington Lincoln Lab., Massachusetts, Rep. no. 582, June 1982.

[28] M. Shchekotov, "Indoor localization method based on Wi-Fi trilateration technique," *Proceeding of the 16th conference of fruct association*, 2014, pp.177–179.

[29] V. Miekk-oja, "Static beacons based indoor positioning method for improving room-level accuracy," M.S. thesis, School of Electrical Eng., Aalto Univ., Helsinki, 2015.[Online]. Available: `https://aaltodoc.aalto.fi/handle/123456789/17724`

[30] O. Motlagh, S. H. Tang, N. Ismail and A. R. Ramli, "A review on positioning techniques and technologies: a novel AI approach," *Journal of Applied Sciences*, vol. 9, no. 9, pp. 1601–1614, 2009.

[31] *The history of the Bluetooth SIG*. Bluetooth SIG. [Online]. Available: `https://www.bluetooth.com/about-us/our-history`

[32] C. Dashevsky, *'So, that's why it's called Bluetooth!' and other surprising tech name origins*. [Online]. Available: `https://www.pcworld.com/article/2061288/so-thats-why-its-called-bluetooth-and-other-surprising-tech-name-origins.html`

[33] D. Tonner, *The bluetooth blues*. [Online]. Available: `https://web.archive.org/web/20071222231740/http://www.information-age.com/article/2001/may/the_bluetooth_blues`

[34] *The right radio, for the right job*. Bluetooth SIG. [Online]. Avaiable: `https://www.bluetooth.com/bluetooth-technology/radio-versions/`

[35] *Bluetooth Low Energy Angle of Arrival (AoA)*, Texas Instruments. [Online]. Available: `http://dev.ti.com/tirex/content/simplelink_academy_cc2640r2sdk_2_40_03_00/modules/blestack/ble_aoa/ble_aoa.html`

[36] *SimpleLink™ Bluetooth® Low Energy CC2640R2F wireless MCU LaunchPad™ development kit* Texas Instruments. [Online]. Available: http://www.ti.com/tool/LAUNCHXL-CC2640R2

[37] Texas Instruments. "Angle of Arrival BoosterPack," [Online]. Available: http://dev.ti.com/BOOSTXL-AOA

[38] F. Belloni, V. Ranki, A. Kainulainen and A. Richter, "Angle-based indoor positioning system for open indoor environments," *2009 6th Workshop on Positioning, Navigation and Communication*, pp. 261–265.

[39] Skyworks Solutions, Inc. "1.0 to 6.0 GHz SP3T Switch," SKY13408-465LF datasheet, Sep. 2015.

[40] Skyworks Solutions, Inc. "0.1 to 3.0 GHz GaAs SPDT Switch," SKY13323-378LF datasheet, Aug. 2017.

[41] Texas Instruments. "SimpleLink™ Angle of Arrival BoosterPack," BOOSTXL-AOA design files, Aug. 2018.

[42] *Localization Toolbox*, Texas Instruments. [Online]. Available: http://dev.ti.com/tirex/content/simplelink_cc2640r2_sdk_2_20_00_49/docs/blestack/ble_user_guide/html/localization/index.html

[43] *RTLS Toolbox*, Texas Instruments. [Online]. Available: http://dev.ti.com/tirex/content/simplelink_cc2640r2_sdk_2_40_00_32/docs/blestack/ble_user_guide/html/ble-stack-3.x-guide/localization-index.html

[44] *boxplot*, Mathworks. [Online]. Available: http://libraryguides.vu.edu.au/ieeereferencing/webbaseddocument

[45] *Box Plots*, NCSS Statistical Software. [Online]. Available: https://ncss-wpengine.netdna-ssl.com/wp-content/themes/ncss/pdf/Procedures/NCSS/Box_Plots.pdf

[46] *BOOSTXL-AOA*, Texas Instruments E2E™ support forums, Feb.28, 2019. [Online]. Available: https://e2e.ti.com/support/wireless-connectivity/other-wireless/f/667/p/777723/2876232?tisearch=e2e-sitesearch&keymatch=BOOSTXL-AOA%20resonance#pi320995filter=all&pi320995scroll=false

LUND
UNIVERSITY

Printed by Tryckeriet i E-huset, Lund 2020

LUND
UNIVERSITY

Series of Master's theses
Department of Electrical and Information Technology
LU/LTH-EIT 2020-748
http://www.eit.lth.se